AD-763 182

INVESTIGATION OF GAGE-PLACEMENT EFFECTS ON A STRESS GAGE EMBEDDED IN GROUT

John Q. Ehrgott

Army Engineer Waterways Experiment Station

Prepared for:

Defense Nuclear Agency

June 1973

MISCELLANEOUS PAPER S-73-37

INVESTIGATION OF GAGE-PLACEMENT EFFECTS ON A STRESS GAGE EMBEDDED IN GROUT

by

J. Q. Ehrgott

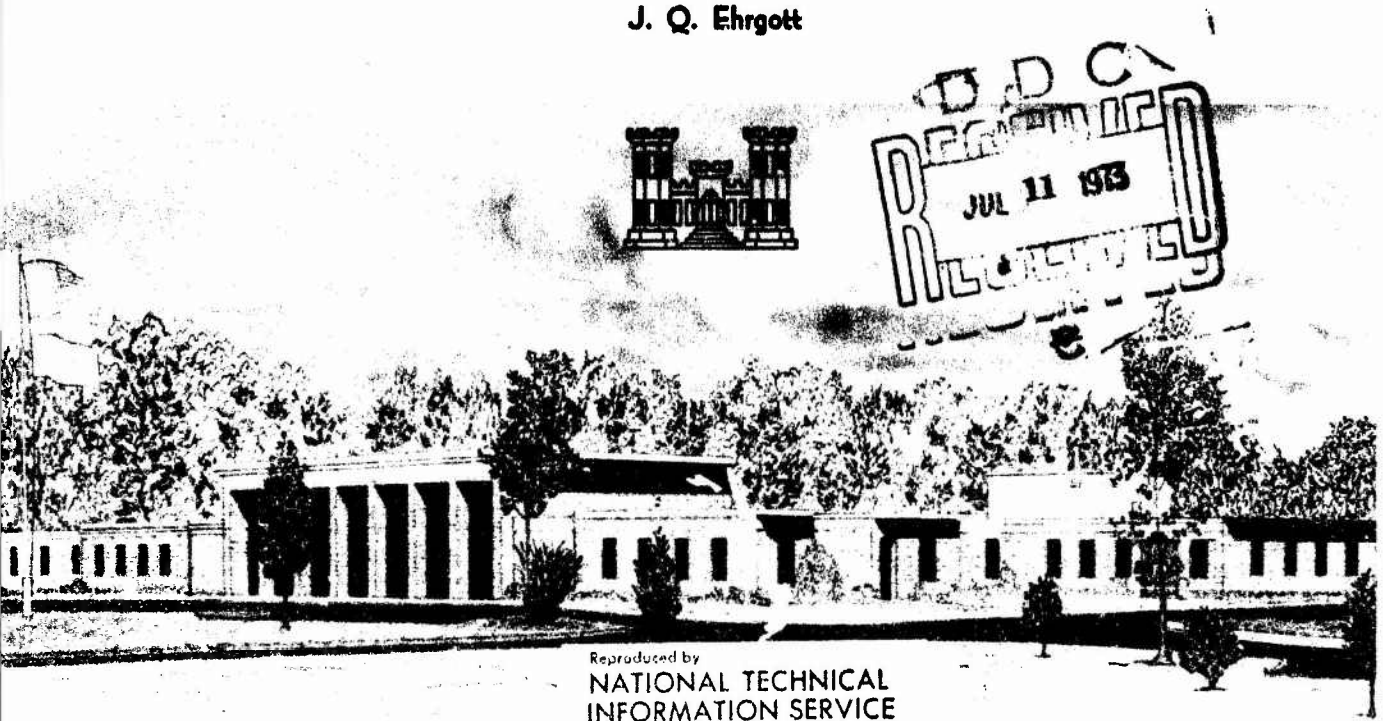

June 1973

Sponsored by Defense Nuclear Agency

Subtask SB209, Work Unit 10, "Laboratory Evaluation of Gage Placement in Field Grout Mixtures"

Conducted by U. S. Army Engineer Waterways Experiment Station
Soils and Pavements Laboratory
Vicksburg, Mississippi

DISCLAIMER NOTICE

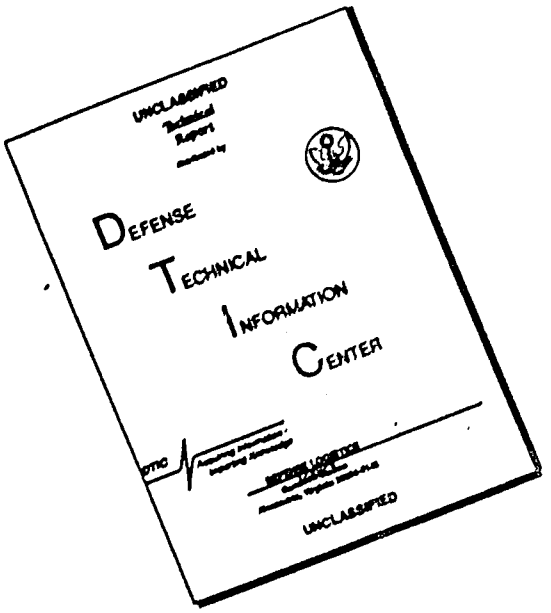

THIS DOCUMENT IS BEST QUALITY AVAILABLE. THE COPY FURNISHED TO DTIC CONTAINED A SIGNIFICANT NUMBER OF PAGES WHICH DO NOT REPRODUCE LEGIBLY.

Unclassified

Security Classification

DOCUMENT CONTROL DATA - R & D

(Security classification of title, body of abstract and indexing annotation must be entered when the overall report is classified)

1. ORIGINATING ACTIVITY (Corporate author) U. S. Army Engineer Waterways Experiment Station Vicksburg, Mississippi	2a. REPORT SECURITY CLASSIFICATION Unclassified 2b. GROUP

3. REPORT TITLE

INVESTIGATION OF GAGE-PLACEMENT EFFECTS ON A STRESS GAGE EMBEDDED IN GROUT

4. DESCRIPTIVE NOTES (Type of report and inclusive dates)

Final report

5. AUTHOR(S) (First name, middle initial, last name)

John Q. Ehrgott

6. REPORT DATE	7a. TOTAL NO. OF PAGES	7b. NO. OF REFS
June 1973	85 75	3

8a. CONTRACT OR GRANT NO.	9a. ORIGINATOR'S REPORT NUMBER(S)
b. PROJECT NO.	Miscellaneous Paper S-73-37
c. Subtask SB209, Work Unit 10	9b. OTHER REPORT NO(S) (Any other numbers that may be assigned this report)
d.	

10. DISTRIBUTION STATEMENT

Approved for public release; distribution unlimited.

11. SUPPLEMENTARY NOTES	12. SPONSORING MILITARY ACTIVITY
	Defense Nuclear Agency, Washington, D. C.

13. ABSTRACT

This report documents a study conducted on the Gulf Radiation Technology (GRT) piezoelectric stress gage in support of the Diamond Mine Event at the Nevada Test Site (NTS). The gage was first calibrated in oil and then embedded in an NTS grout and tested under conditions of uniaxial strain. The results of these tests indicated a slightly nonlinear output of the gage under hydrostatic loadings and an underregistration of the gage when embedded in the grout. Limited uniaxial strain tests were concurrently conducted on the grout mix. The property information from these tests was used as input to the WESTES finite element code in which the test boundary conditions were simulated to analytically investigate behavior of the grout specimen with and without an embedded inclusion or gage. The calculated results indicated that the contact interface between the gage and the grout had the greatest effect on gage performance.

DD FORM 1 NOV 68 1473 REPLACES DD FORM 1473, 1 JAN 64, WHICH IS OBSOLETE FOR ARMY USE.

Unclassified

Security Classification

14 KEY WORDS	LINK A		LINK B		LINK C	
	ROLE	WT	ROLE	WT	ROLE	WT
Computerized simulation						
Grout						
Piezoelectric gages						
Stress gages						
Uniaxial strain tests						

THE CONTENTS OF THIS REPORT ARE NOT TO BE USED FOR ADVERTISING, PUBLICATION, OR PROMOTIONAL PURPOSES. CITATION OF TRADE NAMES DOES NOT CONSTITUTE AN OFFICIAL ENDORSEMENT OR APPROVAL OF THE USE OF SUCH COMMERCIAL PRODUCTS.

ABSTRACT

This report documents a study conducted on the Gulf Radiation Technology (GRT) piezoelectric stress gage in support of the Diamond Mine Event at the Nevada Test Site (NTS). The gage was first calibrated in oil and then embedded in an NTS grout and tested under conditions of uniaxial strain. The results of these tests indicated a slightly nonlinear output of the gage under hydrostatic loadings and an underregistration of the gage when embedded in the grout. Limited uniaxial strain tests were concurrently conducted on the grout mix. The property information from these tests was used as input to the WESTES finite element code in which the test boundary conditions were simulated to analytically investigate behavior of the grout specimen with and without an embedded inclusion or gage. The calculated results indicated that the contact interface between the gage and the grout had the greatest effect on gage performance.

PREFACE

The investigation described in this report was conducted in support of the Diamond Mine Event located at the Nevada Test Site, Mercury, Nevada, and was funded by the Defense Nuclear Agency (DNA). The program was conducted during the period of January 1971 to August 1971. The stress gages used in the study were provided by Gulf Radiation Technology (GRT), a division of Gulf Energy and Environmental Systems, Inc. Dr. Howard Kratz, GRT, provided guidance in the operation of the stress gages.

The investigation was conducted by personnel of the Soils and Pavements Laboratory (S&PL), U. S. Army Engineer Waterways Experiment Station (WES), Vicksburg, Mississippi. The project engineer was Mr. J. Q. Ehrgott, Soil Dynamics Division, S&PL, who also prepared the report, under the supervision of Dr. J. G. Jackson, Jr., Soil Dynamics Division. The various instrumentation circuits used in the evaluation of the stress gages were employed under the direct supervision of Mr. G. C. Downing, Dynamics Branch, Instrumentation Services Division. Dr. N. Radhakrishnan, Computer Analysis Branch, Automatic Data Processing Center, developed the computer code used in the analytical study presented in Appendix B. The rock-matching grout used in the experimental program was supplied by Mr. R. A. Bendinelli, Engineering Mechanics Branch, Concrete Laboratory, who also provided helpful information on the grout material. Mr. P. F. Hadala, Soil Dynamics Division, provided guidance in the analysis of the data. During the conduct of the study Mr. J. P. Sale was Chief of the Soils and Pavements Laboratory. Director of the WES was COL Ernest D. Peixotto, CE, and the Technical Director was Mr. F. R. Brown.

CONTENTS

ABSTRACT---------- 4

PREFACE---------- 5

CONVERSION FACTORS, BRITISH TO METRIC UNITS OF MEASUREMENT---------- 9

CHAPTER 1 INTRODUCTION---------- 10

1.1 Background---------- 10
1.2 Purpose---------- 10
1.3 Scope---------- 10
1.4 Description of the GRT Gage---------- 11

CHAPTER 2 PRELIMINARY TESTS---------- 13

2.1 Description of Laboratory Test Equipment---------- 13
2.2 Comparison with Previous Gage Calibrations---------- 13
2.3 Calibration Checks---------- 14

CHAPTER 3 FIRST TEST SERIES: CALIBRATION OF GAGE---------- 20

3.1 Recording System Used with GRT Gage No. 1---------- 20
3.2 Tests on GRT Gage No. 1---------- 20
3.3 Discussion of Test Results---------- 21
3.4 Results from Tests on GRT Gage No. 3---------- 22

CHAPTER 4 SECOND TEST SERIES: TESTS ON EMBEDDED GAGE---------- 34

4.1 Specimen Preparation---------- 34
4.2 GRT Gage No. 1---------- 35
4.3 GRT Gage No. 3---------- 37

CHAPTER 5 DISCUSSION OF TEST RESULTS---------- 47

5.1 Calibration Tests---------- 47
5.2 Tests on Embedded Gages---------- 47
5.3 Possible Explanations of Test Results---------- 47

CHAPTER 6 CONCLUSIONS AND RECOMMENDATIONS---------- 50

6.1 Conclusions---------- 50
6.2 Recommendations---------- 51

APPENDIX A UNIAXIAL STRAIN TESTS ON GROUT---------- 52

A.1 Material Description---------- 52
A.2 Uniaxial Strain Test Program---------- 53
A.3 Discussion of Test Results---------- 54

APPENDIX B ANALYTICAL STUDY OF FACTORS THAT INFLUENCE GAGE RESPONSE---------- 60

B.1 Background---------- 60
B.2 Purpose---------- 60
B.3 Scope---------- 61
B.4 Description of Study---------- 61

B.5 Code Description---------- 62
B.6 Material Properties---------- 62
B.7 Axial Stress Distribution Within the Grout Specimen--------- 63
B.8 Effect of Gage in the Grout---------- 64
B.9 Effect of a Void Above the Gage---------- 65
B.10 Summary and Conclusions---------- 66

REFERENCES---------- 73

TABLE

2.1 Q-Factors Determined by Several Different Instrumentation Circuits---------- 16

FIGURES

2.1 Cross section of high-pressure uniaxial strain device showing gage location---------- 17
2.2 Calibration of GRT Gage No. 1; peak applied pressure versus output voltage---------- 18
2.3 Calibration of GRT Gage No. 1; Q-factor versus applied pressure---------- 19
3.1 Plot of input increments versus output voltage showing linearity of charge amplifier to scope---------- 23
3.2 Plot of input increments versus output galvanometer travel showing linearity of complete recording system------- 24
3.3 Results of static calibration of GRT Gage No. 1---------- 25
3.4 Tracing of oscillograph record from Test GA-1---------- 26
3.5 Tracing of oscillograph record from Test GA-2---------- 27
3.6 Tracing of oscillograph record from Test GA-3---------- 28
3.7 Tracing of oscillograph record from Test GA-4---------- 28
3.8 Tracing of oscillograph record from Test GA-5---------- 29
3.9 Tracing of oscillograph record from Test GA-6---------- 30
3.10 Tracing of oscillograph record from Test GA-7---------- 31
3.11 Results of seven dynamic calibration tests conducted on GRT Gage No. 1---------- 32
3.12 Results of seven dynamic calibration tests conducted on GRT Gage No. 3---------- 33
4.1 Tracing of oscillograph record from Test GA-1-1---------- 39
4.2 Tracing of oscillograph record from Test GA-1-2---------- 39
4.3 Tracing of oscillograph record from Test GA-1-3---------- 40
4.4 Tracing of oscillograph record from Test GA-1-4---------- 40
4.5 Tracing of oscillograph record from Test GA-1-5---------- 41
4.6 Tracing of oscillograph record from Test GA-1-6---------- 41
4.7 Tracing of oscillograph record from Test GA-1-7---------- 42
4.8 Calibration curves of GRT Gages No. 1 and 3---------- 43
4.9 Results of seven dynamic tests conducted on GRT Gage No. 1 embedded in grout---------- 44
4.10 Tracing of oscillograph record from Test GA-2-1---------- 45
4.11 Results of one dynamic test conducted on GRT Gage No. 3 embedded in grout---------- 46
A.1 Uniaxial strain test results on grout, 15-day cure time----- 56
A.2 Uniaxial strain test results on grout, 16-day cure time----- 57

A.3 Uniaxial strain test results on grout, 20-day cure time------ 58
A.4 Uniaxial strain test results on grout, 13-day cure time------ 59
B.1 Cross section of special grout specimen with embedded GRT gage---------- 68
B.2 Half section of grout and gage as idealized for finite element code---------- 68
B.3 Half section of grout specimen showing elements of interest-- 69
B.4 Plot of axial stress versus location of elements showing axial stress distribution across specimen at four elevations---------- 69
B.5 Half section of specimen with actual location of GRT gage showing limit of sidewall friction on axial stress distribution across specimen---------- 70
B.6 Results of Cases I and II plotted as axial stress versus element location for elevation directly above gage---- 71
B.7 Results of Cases III and IV plotted as axial stress versus element location for elevation directly above gage---------- 72

CONVERSION FACTORS, BRITISH TO METRIC UNITS OF MEASUREMENT

British units of measurement used in this report can be converted to metric units as follows:

Multiply	By	To Obtain
mils	0.0254	millimeters
inches	2.54	centimeters
pounds (force) per square inch	0.6894757	newtons per square centimeter
kips (force) per square inch	0.6894757	kilonewtons per square centimeter
picocoulombs per pounds (force) per square inch	0.6894757	picocoulombs per newtons per square centimeter
pounds (mass) per cubic foot	16.0185	kilograms per cubic meter
feet per second	0.3048	meters per second

CHAPTER 1

INTRODUCTION

1.1 BACKGROUND

The U. S. Army Engineer Waterways Experiment Station (WES) was requested by the Defense Nuclear Agency (formerly the Defense Atomic Support Agency) to conduct three separate laboratory investigations in support of the Diamond Mine Event located at the Nevada Test Site (NTS). The investigations included: (1) determination of the effect of the rate of loading on laboratory constitutive properties of tuff, (2) development of an improved rock-matching grout, and (3) evaluation of gage-placement effects on a stress gage embedded in a grout medium. This report covers Study 3. The others are being separately reported.

1.2 PURPOSE

One of the measurement systems used in underground explosive field tests is a stress gage embedded in a grout core. It is used to provide a direct measure of the stress pulse propagating through the earth media during an event. One such gage is the piezoelectric, earth-pressure and concrete-pressure stress gage developed by Gulf Radiation Technology (GRT) called the GRT gage. The unit is precalibrated in the laboratory, generally under a known hydrostatic loading. The gage is then embedded in a special grout plug, which is placed in a drill hole in the field at a preselected location and grouted in place. The data that are generated by the gage during the field event are interpreted by use of the laboratory-obtained gage calibration. The purpose of this study was to determine if the GRT stress gage's output is affected when embedded in a grout plug subjected to a state of uniaxial strain under controlled laboratory conditions.

1.3 SCOPE

The investigation consisted of two series of tests conducted on two separate GRT gages in the WES high-pressure uniaxial strain device. The

first test series consisted of calibration of the GRT gages in a fluid environment under a variety of pressure levels and loading pulses. The gages were placed in a grout specimen, a procedure similar to the practice of placing the gage in a grout plug in a borehole for use in a field test, and the second series of tests was then conducted on the grout specimens containing the precalibrated GRT gages. Preselected stress pulses were applied through a fluid to the top surface of the grout specimen, and the applied surface stress pulse and the pulse measured by the embedded GRT gage were simultaneously recorded while the specimen was maintained in a state of uniaxial strain (i.e., no radial strain was permitted).

This report documents the results from the two test series. The test series are described, and tracings are presented of the oscillograph records that show the output of both the GRT gage and the pressure transducer used to measure the applied pulse. Results of uniaxial strain tests conducted on the grout mix used in this investigation are given in Appendix A. An analytical investigation using a finite element code was also conducted, and the results are presented in Appendix B.

1.4 DESCRIPTION OF THE GRT GAGE

The GRT gage is a small, approximately 0.7-inch[1]-diameter by 0.3-inch-thick stainless steel body containing a 3/8-inch-diameter piezoelectric crystal which is sandwiched between two layers of ceramic and has a thin, 0.02-inch-thick diaphragm of stainless steel. Stainless steel tubing is connected to the body of the unit and protects the electrical wire which passes through the body to the crystal. The entire gage body, including the gage face with diaphragm, is covered with a thin coat of epoxy that waterproofs the gage.

The GRT gages received by WES differed from the gages used in the field in that the stainless steel tubing protecting the electrical wires

---

[1] A table of factors for converting British units of measurement to metric units is presented on page 9.

was shortened to approximately 3 inches. The tube was also filled with epoxy, which allowed the entire gage to be placed in the WES high-pressure uniaxial strain device and loaded hydrostatically in oil.

CHAPTER 2

PRELIMINARY TESTS

2.1 DESCRIPTION OF LABORATORY TEST EQUIPMENT

All the laboratory tests were conducted in the WES high-pressure uniaxial strain test device (HP 1-D). This device consists of a fluid container, containing the fluid chamber and pressure transducer, and a base, which contains the soil chamber. Load from a dynamic loading machine or ram loader can be transmitted to the piston in the fluid chamber which compresses the fluid to produce the pressure pulse. Controlled-load rise times as fast as 3 msec and decay times as fast as 20 msec can be produced.

Figure 2.1 shows a cross section of the HP 1-D with the GRT gage and the WES internal pressure cell located in the base, which was filled with fluid for these tests. In the dynamic tests and in some static tests, the pressure in the chamber was produced by the load from the dynamic loading machine. In some static calibration tests, the pressure was produced by an Ashcroft portable deadweight tester, Type 1305-B, connected to a port located in the piston of the HP 1-D.

The output voltage signals from the two WES pressure transducers are converted by a carrier amplifier to proportional output current signals, which drive galvanometers in an oscillograph that then record the data on light-sensitive paper. One-msec timing marks produced by a precision oscillator can be recorded on the paper. The basic circuit of the GRT gage consists of a charge amplifier and operational amplifier, which allow its output to also be recorded in the oscillograph. In some tests, an oscilloscope was connected to the output of the charge amplifier to record the peak voltage during a test.

2.2 COMPARISON WITH PREVIOUS GAGE CALIBRATIONS

The calibration of the GRT piezoelectric gage can be expressed in terms of a charge sensitivity or Q-factor as

$$Q = \frac{(v/P)\ C}{1{,}000} \qquad (2.1)$$

where Q = charge sensitivity, picocoulombs/psi

v = output voltage, millivolts

P = pressure on the gage, psi

C = circuit capacitance, picofarads

From the above equation, it is evident that the specifications of a constant Q-factor for a gage imply a linear relation of gage output to pressure. A Q-factor of 113.7 picocoulombs/psi was supplied to WES by GRT for use with the gages. Initial WES check tests did not confirm this Q-factor; therefore, some preliminary studies of the gage's calibration were conducted.

2.3 CALIBRATION CHECKS

A series of calibration check tests using a variety of dynamic (3- to 50-msec) and static (1- to 2-minute) rise times was conducted at WES in the HP 1-D. The gage was connected to a Kistler Model 565-86 charge amplifier, and the peak voltage was measured at peak pressure. The results of these tests are shown in Figure 2.2 as a plot of peak applied pressure versus output voltage. Superimposed on the plot of the measured data points is a plot of the relation of pressure versus voltage which should have been measured based on the GRT Q-factor of 113.7 picocoulombs/psi. At low pressures (less than 3 ksi), the curves agree fairly well; however, at higher pressures, the WES measured values indicate that the gage output is slightly nonlinear.

In addition to the above-mentioned tests, another series was conducted at WES using the circuit mentioned above and four other instrumentation circuits. These five circuits were as follows: (1) the gage connected to a charge amplifier, Kistler Model 565-86, (2) the gage connected directly to an oscilloscope, Hewlett Packard Model 502A, (3) the gage connected to an operational amplifier, Analog Device Model 147 B, used as a high-input impedance voltage amplifier, (4) the gage connected to an operational amplifier, Analog Device Model 147 B, used as a charge

amplifier, and (5) the gage connected to a charge amplifier, Kistler Model 503-M5. Table 2.1 lists the type circuit, selected values of applied pressure, and the calculated charge sensitivity factor. Note that in some of the tests, the CRT gage polarity was reversed. Figure 2.3 is a plot of the data in Table 2.1 in the form of the Q-factor versus applied pressure.

Based on the results listed in Table 2.1 and the results shown in Figures 2.2 and 2.3, it appears that the Q-factor varies from approximately 114 picocoulombs/psi at the lower pressures to approximately 135 picocoulombs/psi at 5,000 psi and higher pressures and that the gage response is nonlinear. The type of amplifier or circuit used does not appear to have any effect that exceeds normal data scatter, which can be related to the resolution of the oscilloscope used to monitor voltage.

TABLE 2.1 Q-FACTORS DETERMINED BY SEVERAL DIFFERENT INSTRUMENTATION CIRCUITS

Type Circuit	Applied Pressure	Calculated Charge Sensitivity Q-Factor
	psi	picocoulombs/psi
Gage to charge amplifier, Kistler Model 565-S6	1,025	115
	2,025	120
	5,025	134
Gage to oscilloscope, Hewlett Packard Model 502A	1,000	115
	4,300[a]	122.5-129[a]
	8,050[b]	137.5
	8,200[b]	135.0
Gage to high-input impedance voltage amplifier, Analog Device Model 147 B	3,025[b]	120
	3,025[b]	120
	5,025[b]	132
	5,025[b]	138
Gage to charge amplifier, Analog Device Model 147 B	3,025[b]	120
	5,025[b]	135
Gage to charge amplifier, Kistler Model 503-M5	1,025	117
	2,025	121
	3,025	129

[a] Twenty-two-msec rise time; therefore, assumed 90 and 86 percent of measured peak voltage to bound voltage loss due to rise time.

[b] Polarity reversed--red wire to shield.

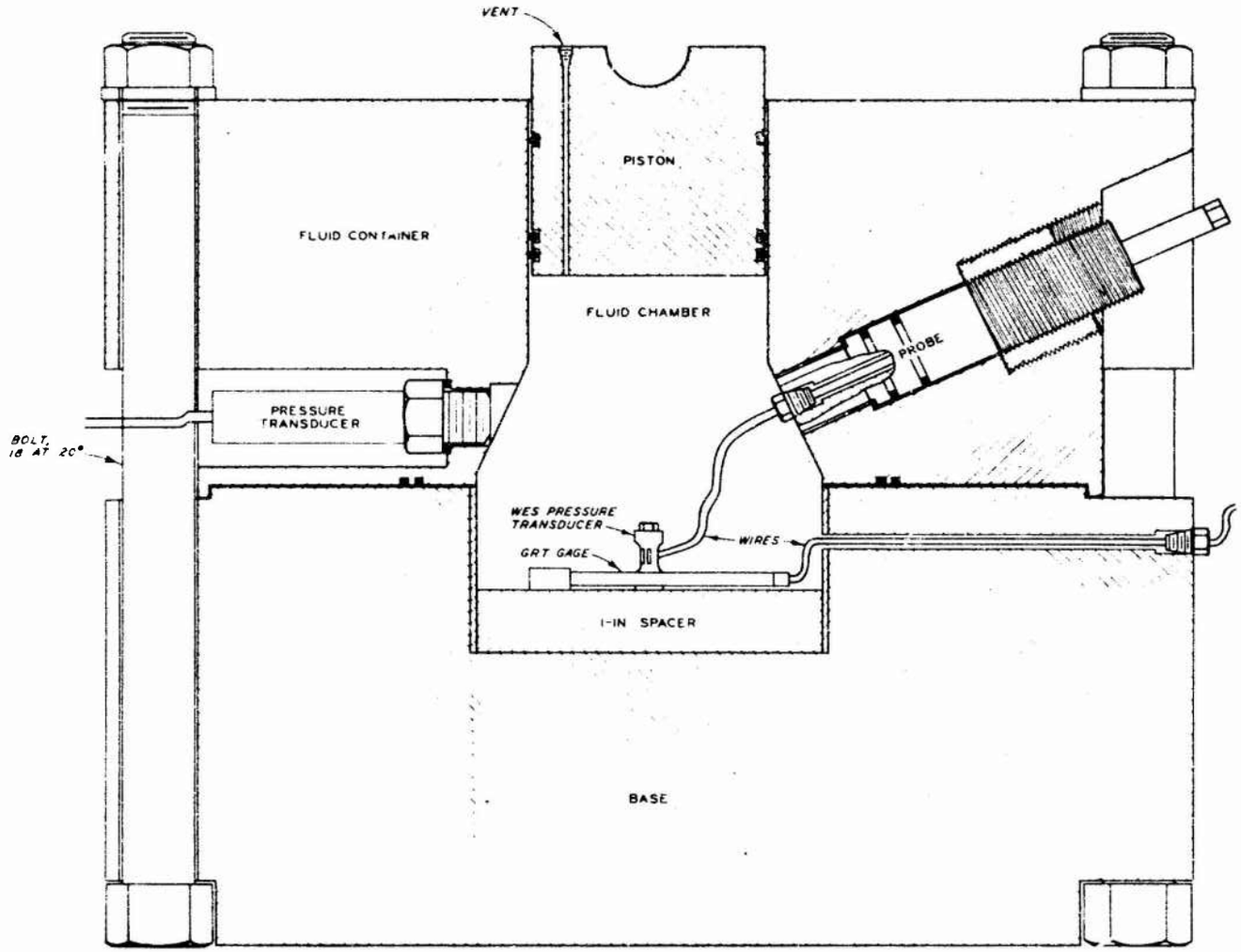

Figure 2.1 Cross section of high-pressure uniaxial strain device showing gage location.

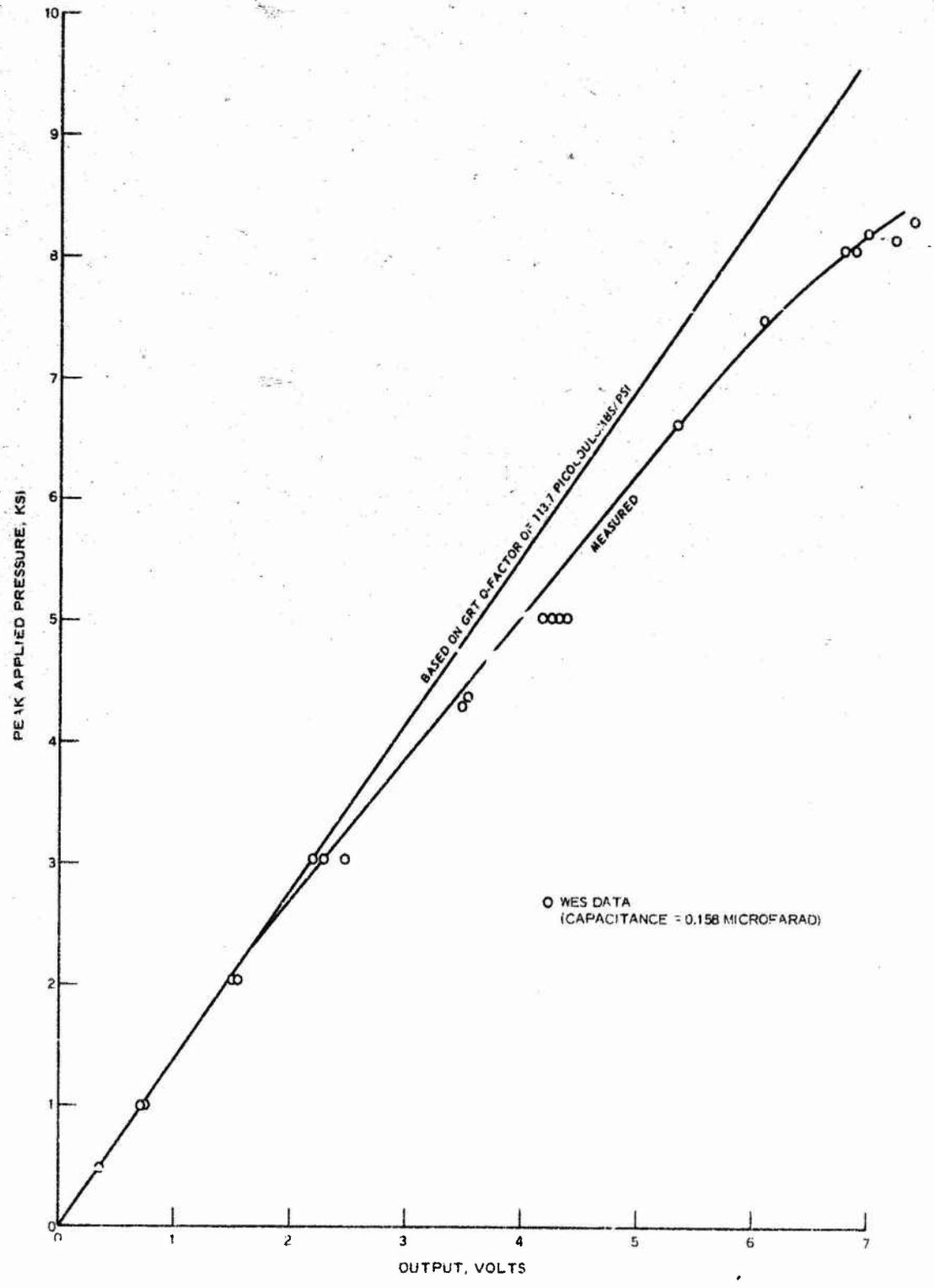

Figure 2.2 Calibration of GRT Gage No. 1. Peak applied pressure versus output voltage.

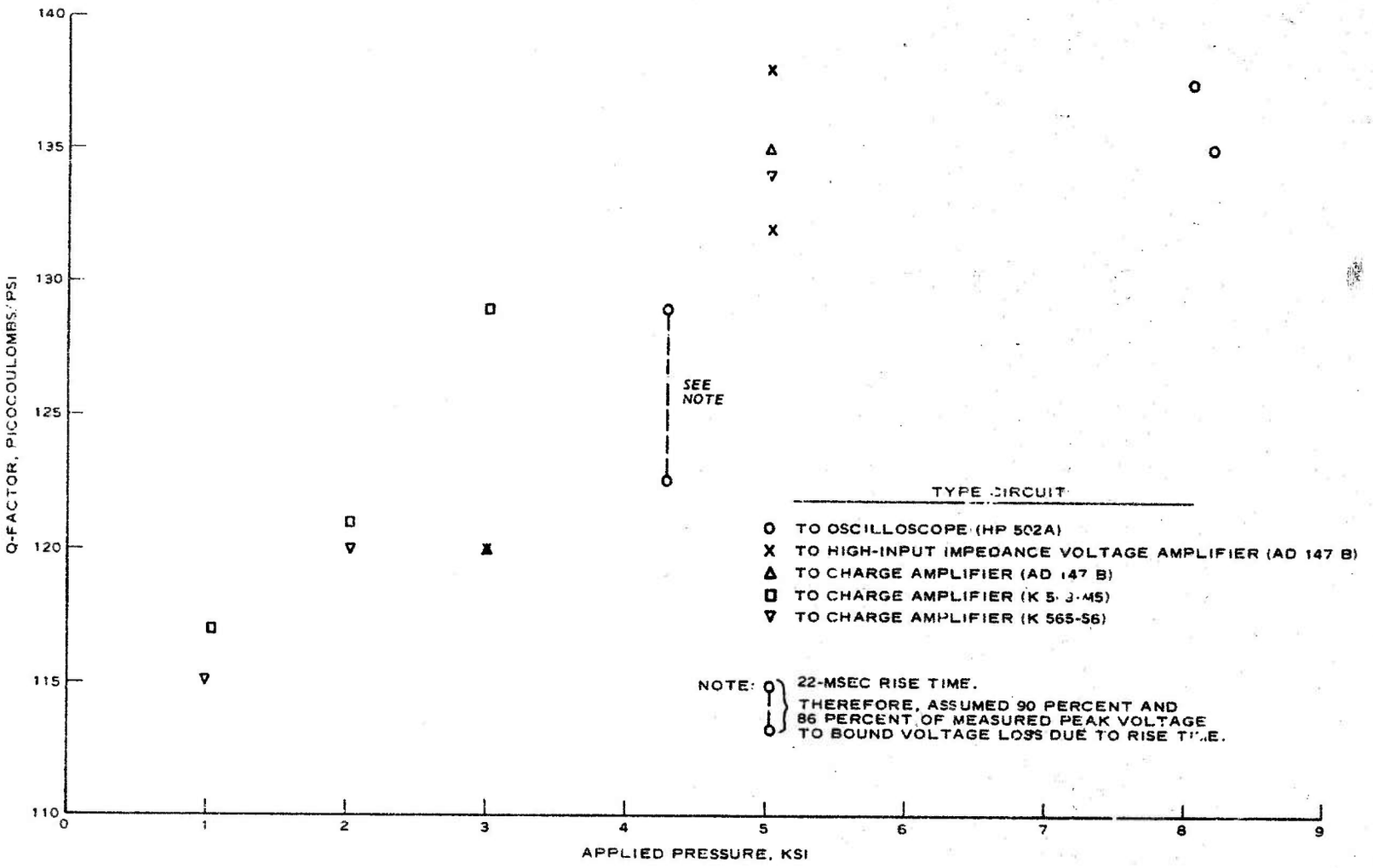

Figure 2.3 Calibration of GRT Gage No. 1. Q-factor versus applied pressure.

CHAPTER 3

FIRST TEST SERIES: CALIBRATION OF GAGE

Initially, one gage was received from GRT. All the preliminary testing and most of the tests of the first test series presented in this chapter were conducted on the first gage (GRT Gage Serial No. 1). Another gage (GRT Gage Serial No. 3) was received by WES just prior to the second test series. Rather than conducting a separate test series on GRT Gage Serial No. 3, it was placed in the fluid container of the high-pressure uniaxial strain device and tested in oil during the test series in which GRT Gage No. 1 was embedded in a grout specimen. The pressure-voltage curves from the test of GRT Gage No. 3 in oil were similar to those for Gage No. 1 in oil. In this chapter, only the results from the tests on GRT Gage No. 1 in oil will be discussed.

3.1 RECORDING SYSTEM USED WITH GRT GAGE NO. 1

The first test series was conducted on GRT Gage No. 1 using the WES pressure transducer as a standard. The circuit using the Kistler Model 565-S6 charge amplifier was used in both test series. Figure 3.1 shows a plot of applied equal increments of voltage versus measured output of the charge amplifier indicating the linearity of the amplifier for voltages less than 10 volts. Figure 3.2 shows the results of a linearity check conducted on the complete amplifier and recording system as recorded on the oscillograph. The plot shows the applied equal increments of voltage versus the measured deflection of the trace on the oscillograph recording paper and indicates linearity for up to 4 inches of galvanometer travel. It should be noted that the polarity of the gage did not appear to affect the measured results. Therefore, the gage polarity was reversed to be compatible with the preferred polarity of the instrumentation circuit used to record the output on the oscillograph.

3.2 TESTS ON GRT GAGE NO. 1

A static calibration was first conducted by applying known pressure

with the deadweight tester to the oil around the GRT gage and recording the gage output on the oscillograph. Figure 3.3 shows the plot of applied pressure versus galvanometer travel on the oscillograph recording paper. Note that the same trend in nonlinearity is seen in this plot as was seen in Figure 2.2. Figures 3.4 through 3.10 are tracings of the actual oscillograph records from each of the dynamic tests showing the output of GRT Gage No. 1 and the two WES pressure transducers.

3.3 DISCUSSION OF TEST RESULTS

GRT Gage No. 1 and the circuit used were found to be very stable and drift-free throughout the test duration. The output of the gage was repeatable. In one test (Test GA-6), the applied peak pressure of 10,500 psi caused electrical saturation of the charge amplifier; however, the GRT gage continued to track the pulse oscillations once the pressure fell below the saturation level (10 to 11 volts maximum). In all of the tests, the gage gave results consistent with those results obtained during the preliminary test series.

It should be noted that there is a time delay inherent in the carrier amplifier used with the two WES pressure transducers that is not inherent in the charge amplifier. As a result, there is a 1/4-msec time shift between the GRT gage's output when compared with the WES transducer output recorded on the oscillograph. The delay is apparent only on those tests with very fast (3 msec) rise times but is easily corrected for in the data reduction of the oscillograph record.

Randomly selected data points from each of the tests are shown in Figure 3.11 as a plot of pressure, determined from the WES pressure transducer, versus galvanometer travel, determined from the output of GRT Gage No. 1. Except for the first two tests, which had a different electrical gain, the data points describe a slightly nonlinear calibration curve. This calibration plot was used to interpret the output of Gage No. 1 on the oscillograph records from the second series tests to be presented in the next chapter.

3.4 RESULTS FROM TESTS ON GRT GAGE NO. 3

As mentioned previously, the first or calibration test series on GRT Gage No. 3, which was conducted to calibrate the gage in a fluid environment, was conducted simultaneously with the second test series on GRT Gage No. 1 embedded in a grout specimen. The output of the WES pressure transducer and GRT Gage No. 3, both located in the fluid container of the uniaxial strain device, and the output of GRT Gage No. 1 embedded in a grout specimen were recorded. Tracings of the oscillograph records will be presented in Chapter 4. The results indicate that the response of this gage is also nonlinear; however, the actual voltage output from GRT Gage No. 3 was not monitored during these tests. The gage was repeatable and stable during all the tests. Figure 3.12 presents the calibration curve for Gage No. 3 as a plot of pressure, as determined from the WES pressure transducer, versus the oscillograph galvanometer travel for Gage No. 3 when it was located in the pressurized oil. This curve is also slightly nonlinear.

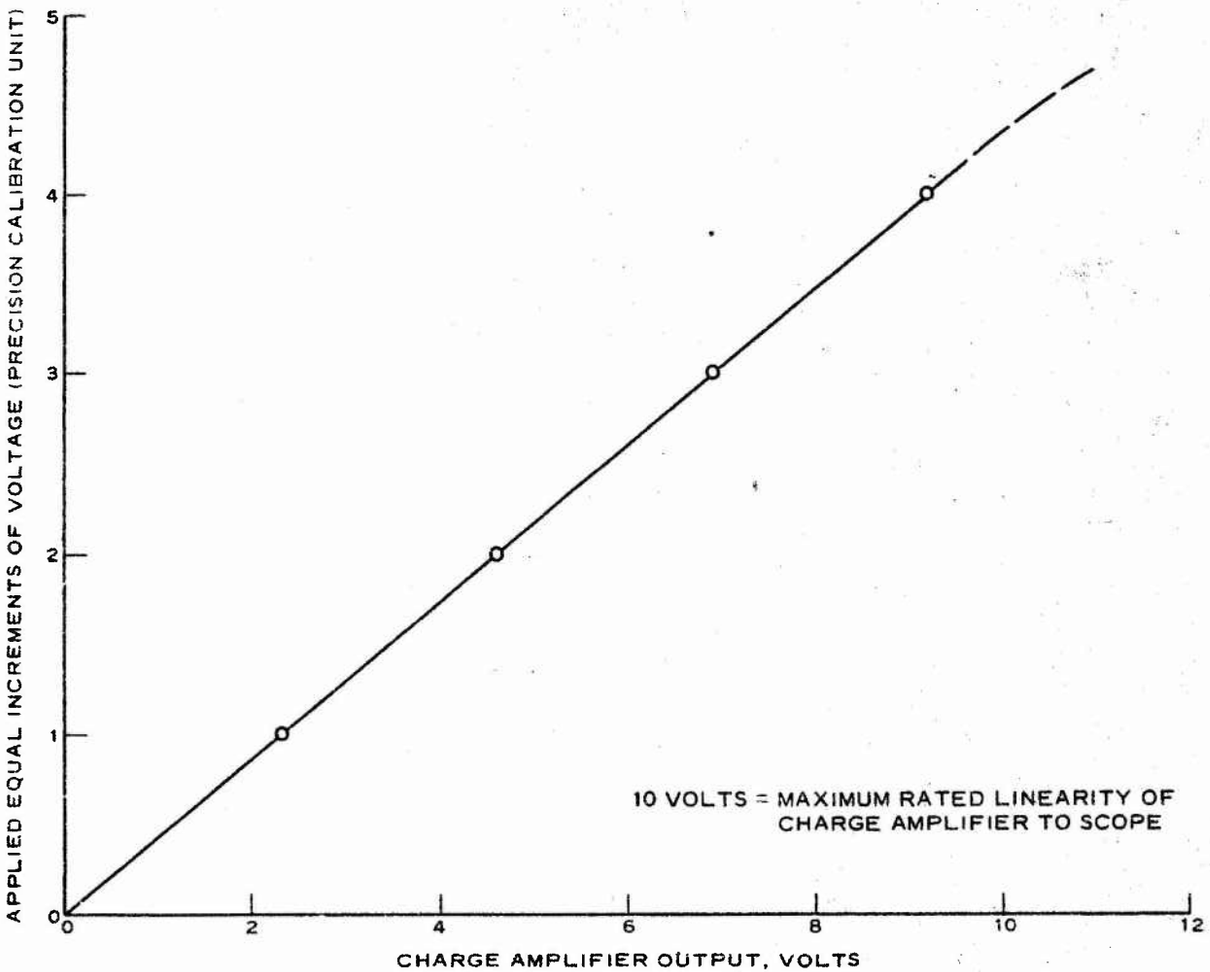

Figure 3.1 Plot of input increments versus output voltage showing linearity of charge amplifier to scope.

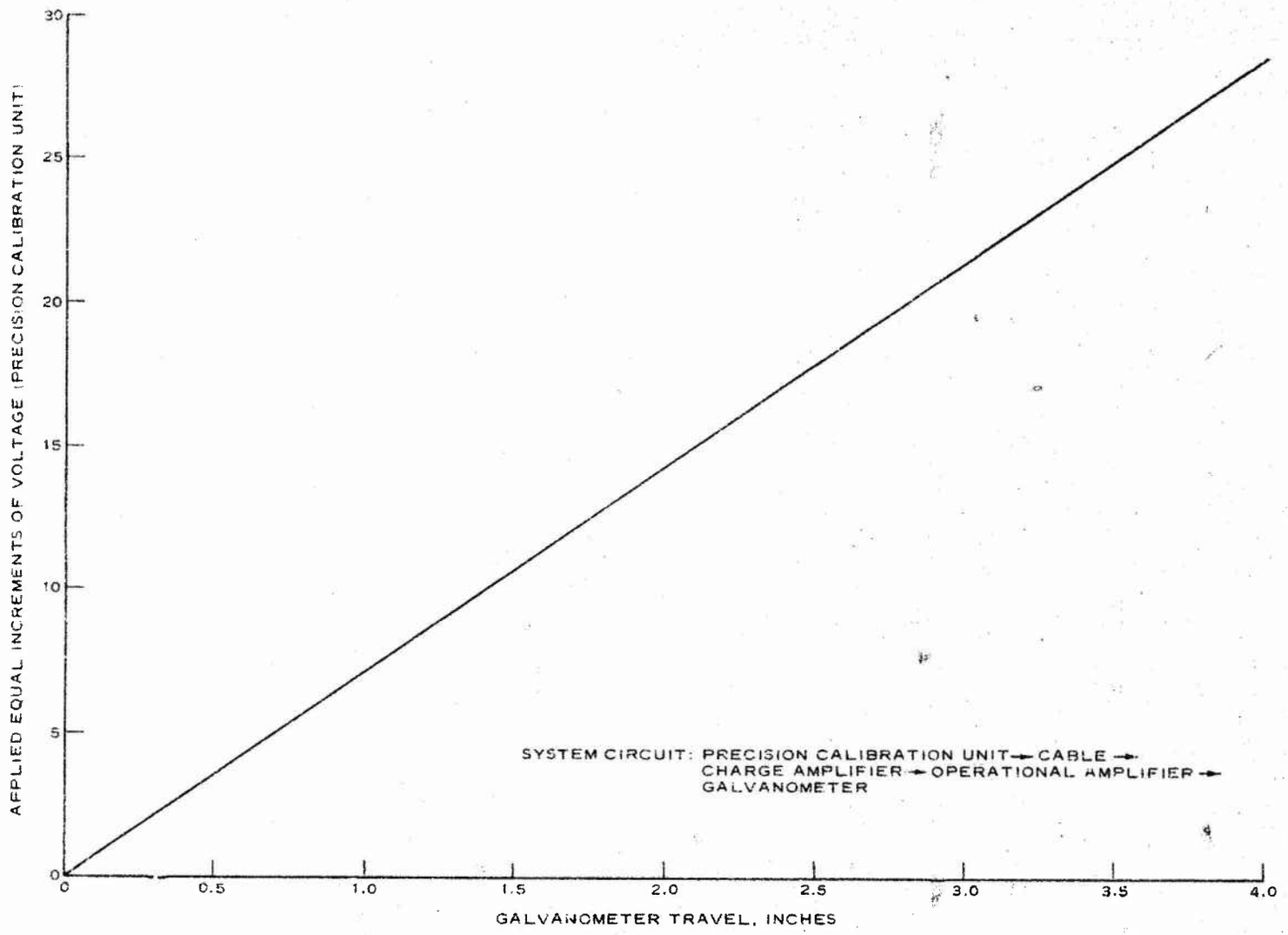

Figure 3.2 Plot of input increments versus output galvanometer travel showing linearity of complete recording system.

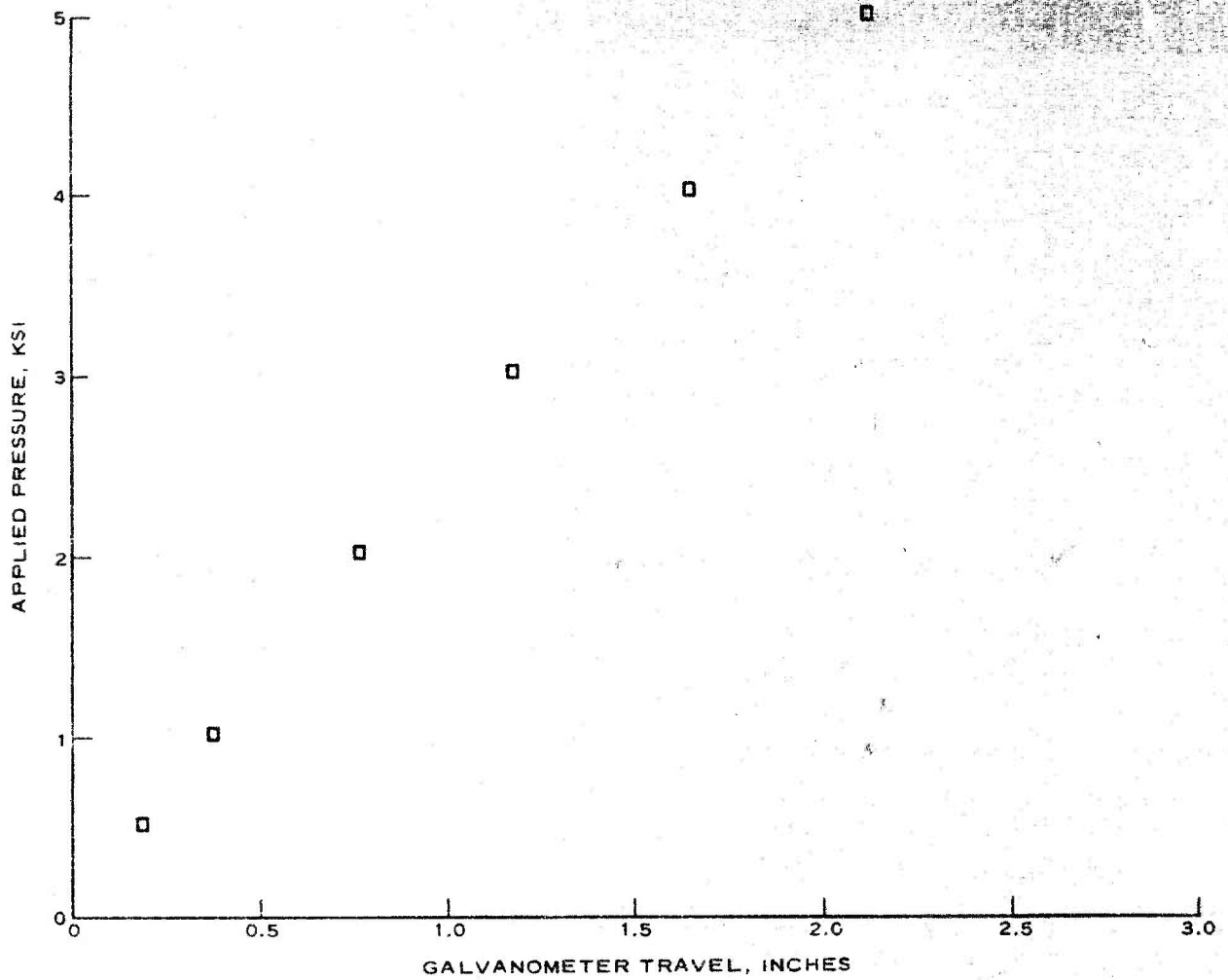

Figure 3.3 Results of static calibration of GRT Gage No. 1.

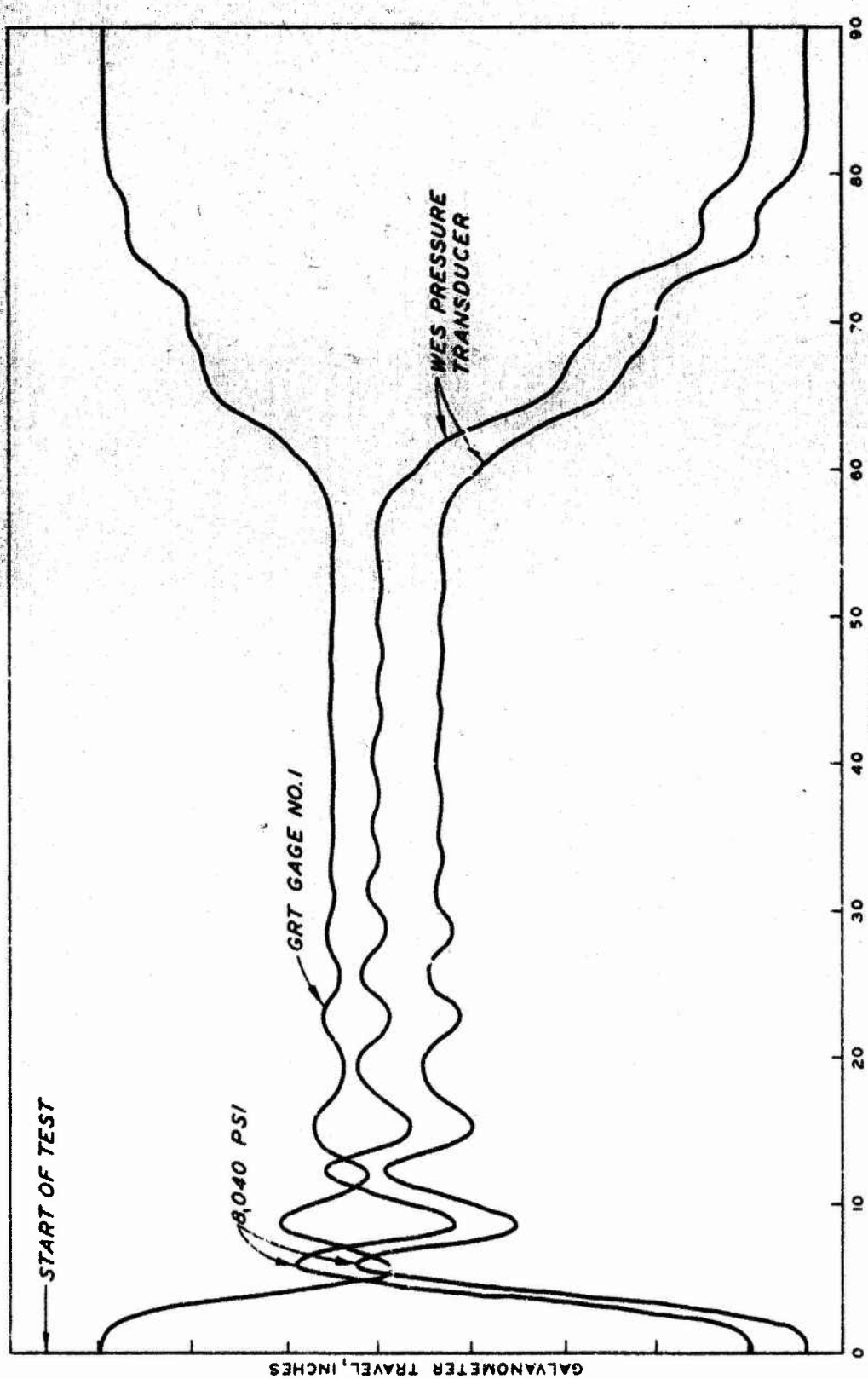

Figure 3.4 Tracing of oscillograph record from Test GA-1.

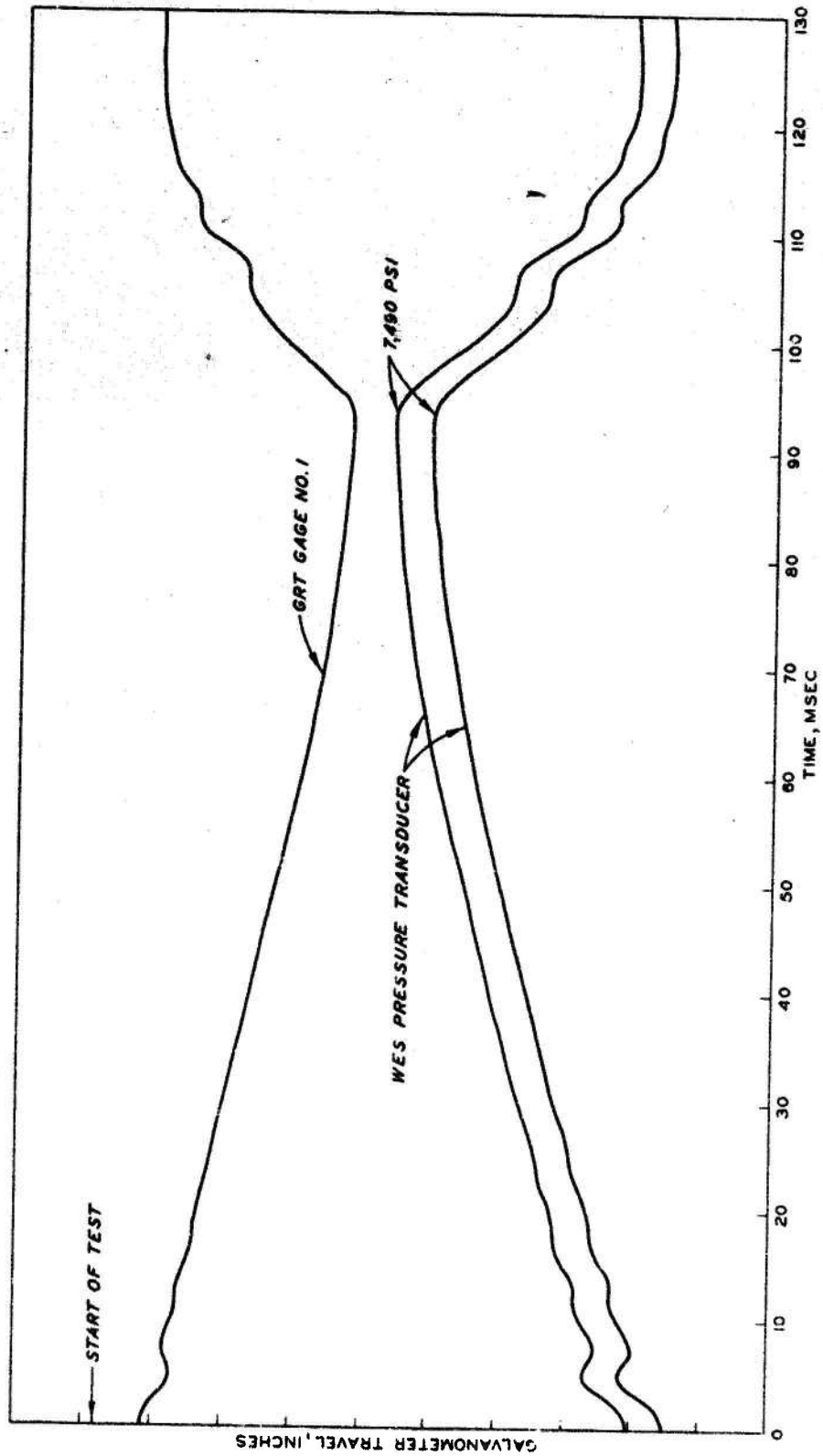

Figure 3.5 Tracing of oscillograph record from Test GA-2.

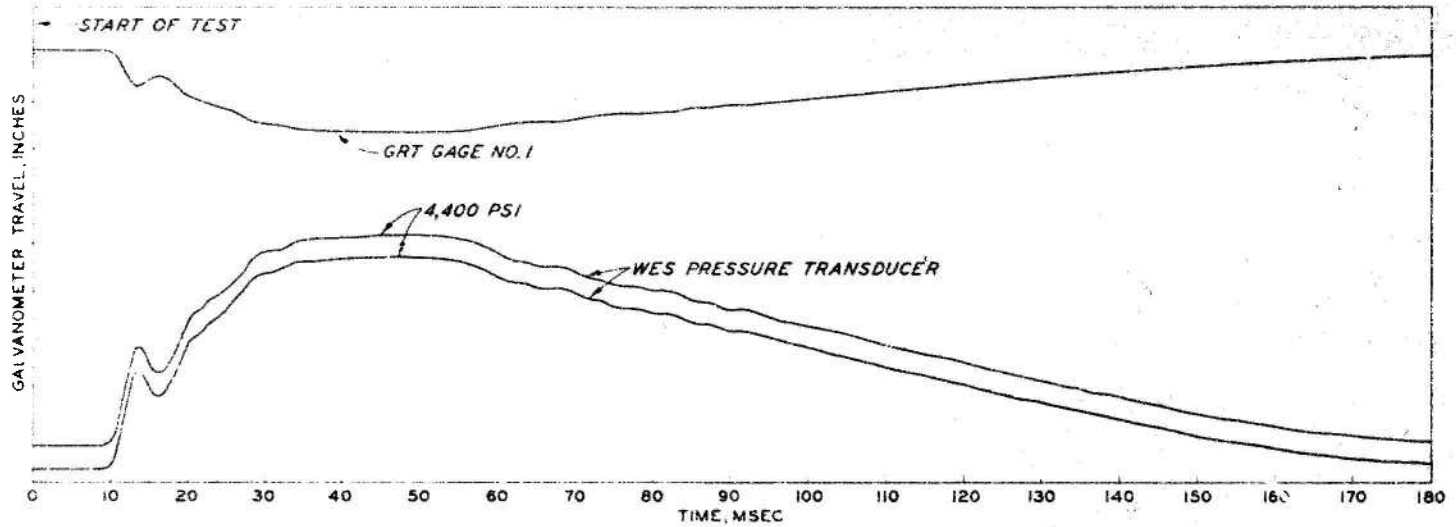

Figure 3.6 Tracing of oscillograph record from Test GA-3.

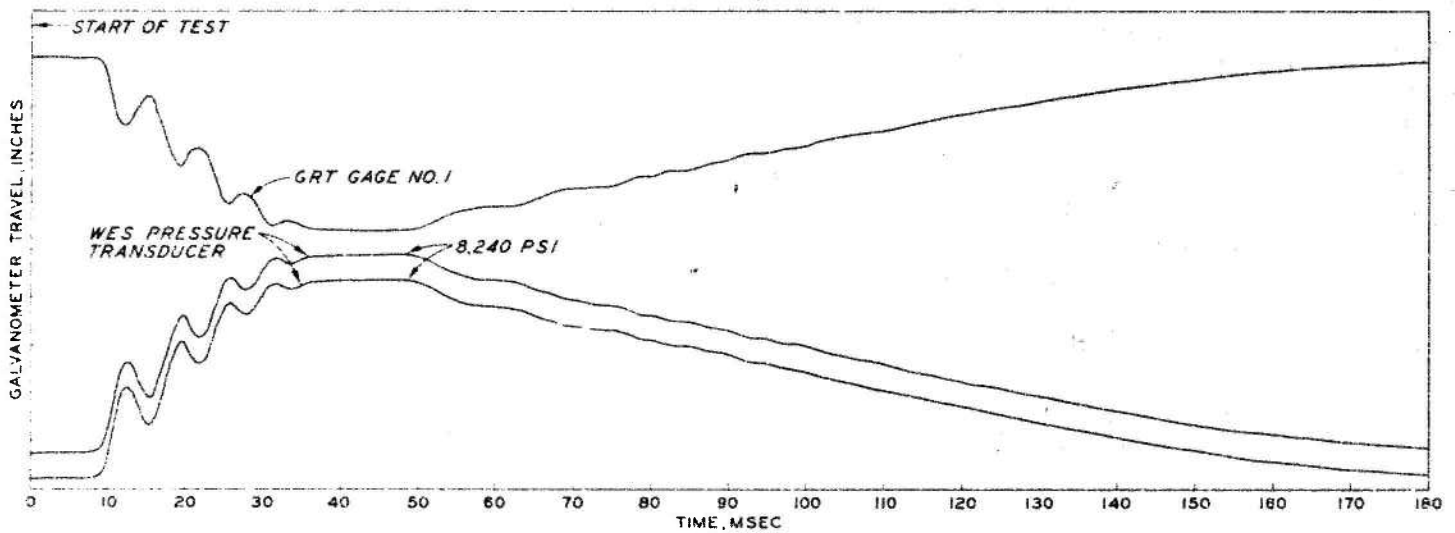

Figure 3.7 Tracing of oscillograph record from Test GA-4.

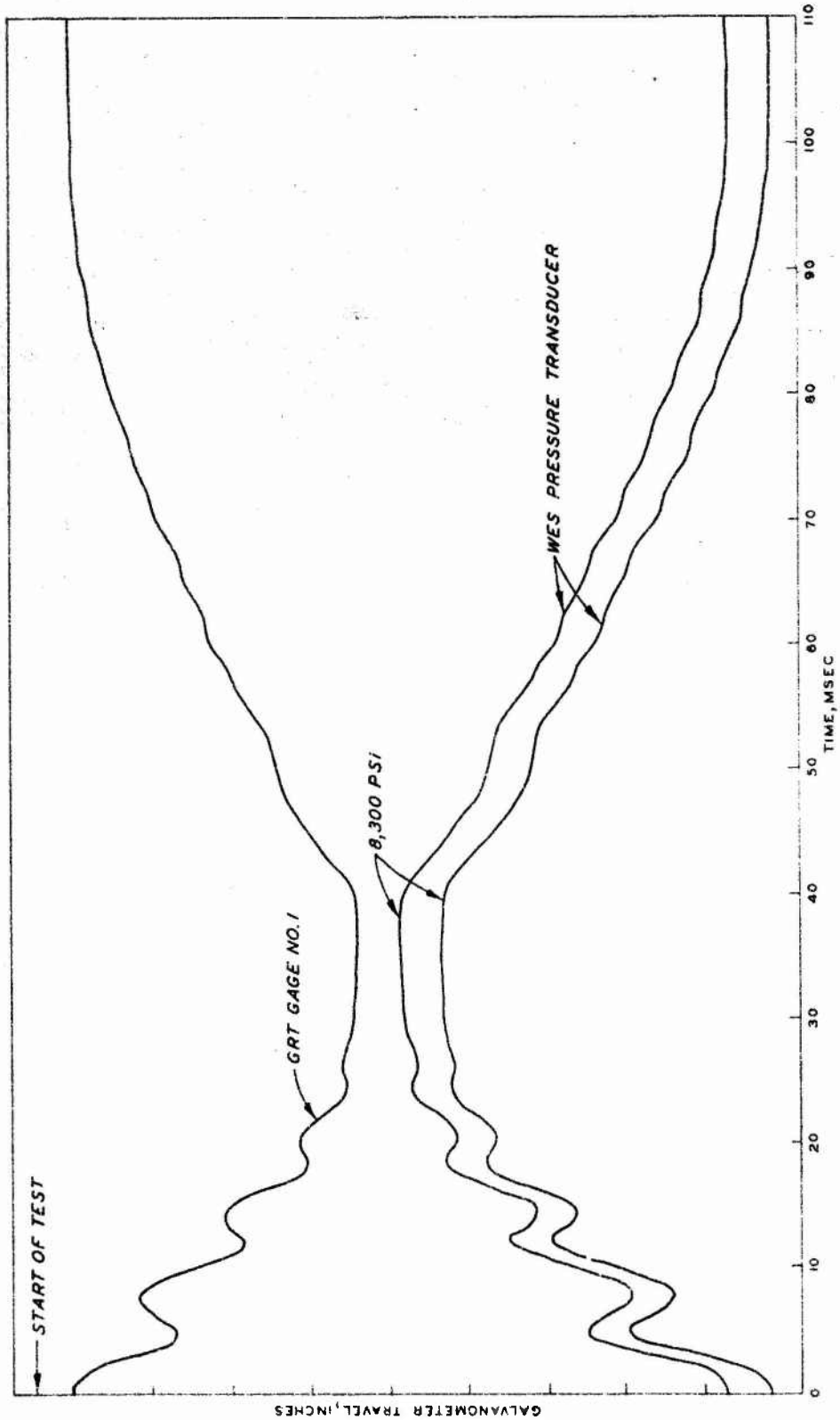

Figure 3.8 Tracing of oscillograph record from Test GA-5.

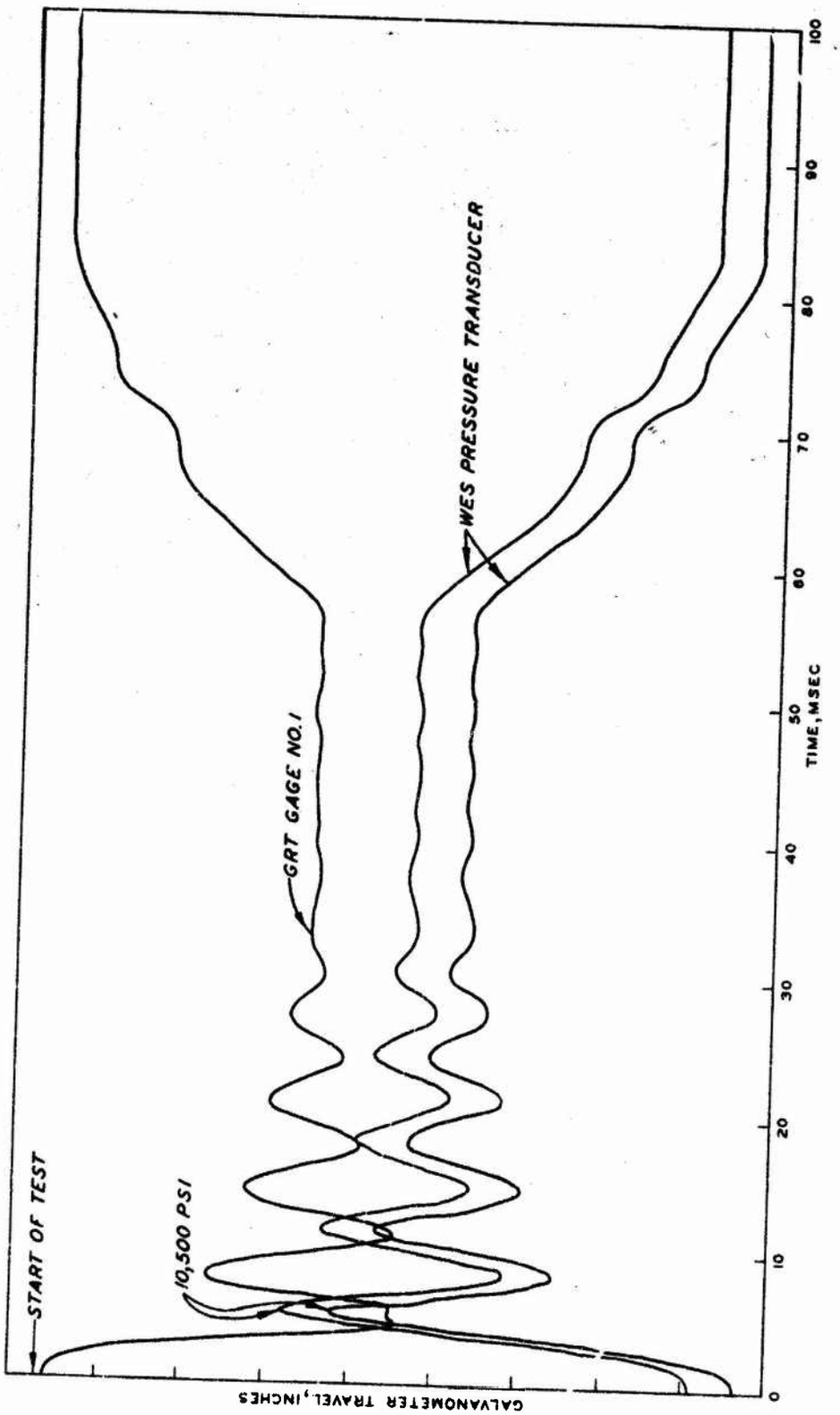

Figure 3.9 Tracing of oscillograph record from Test GA-6.

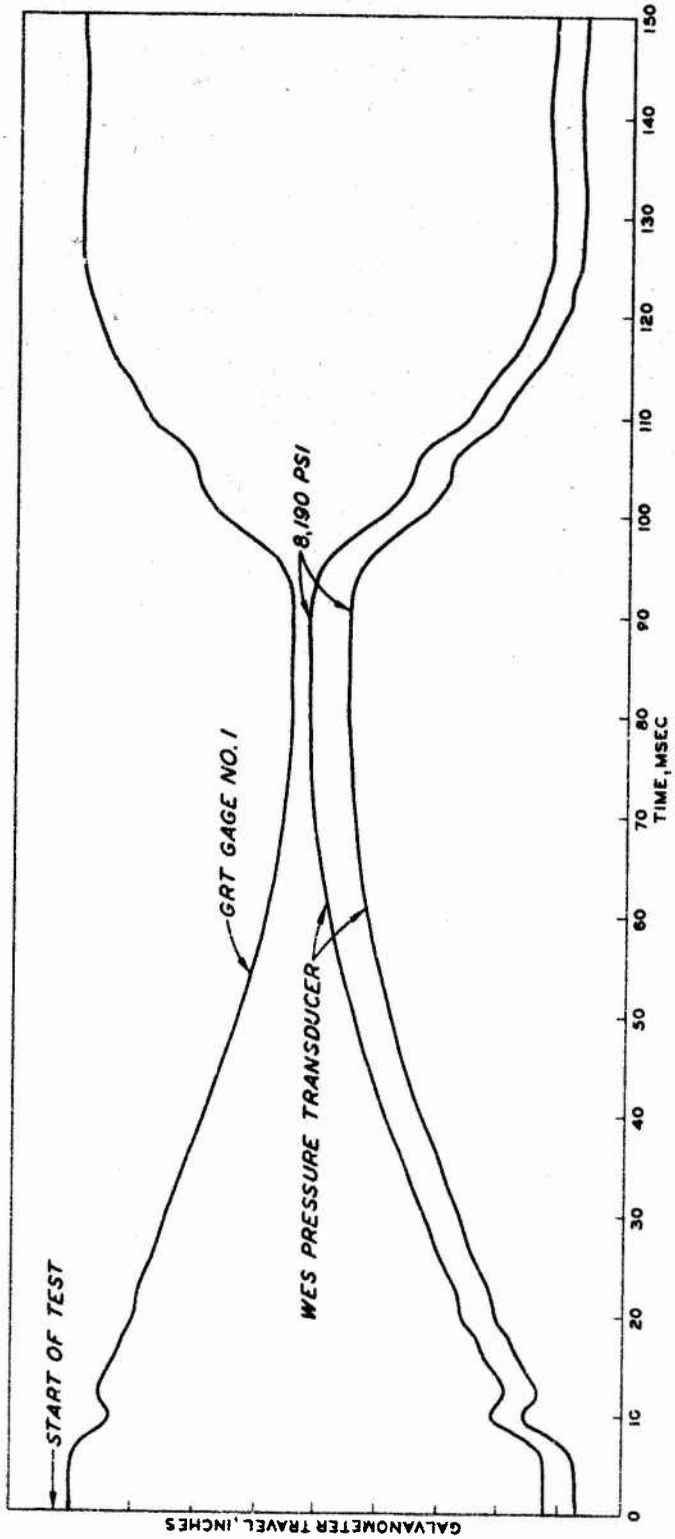

Figure 3.10 Tracing of oscillograph record from Test GA-7.

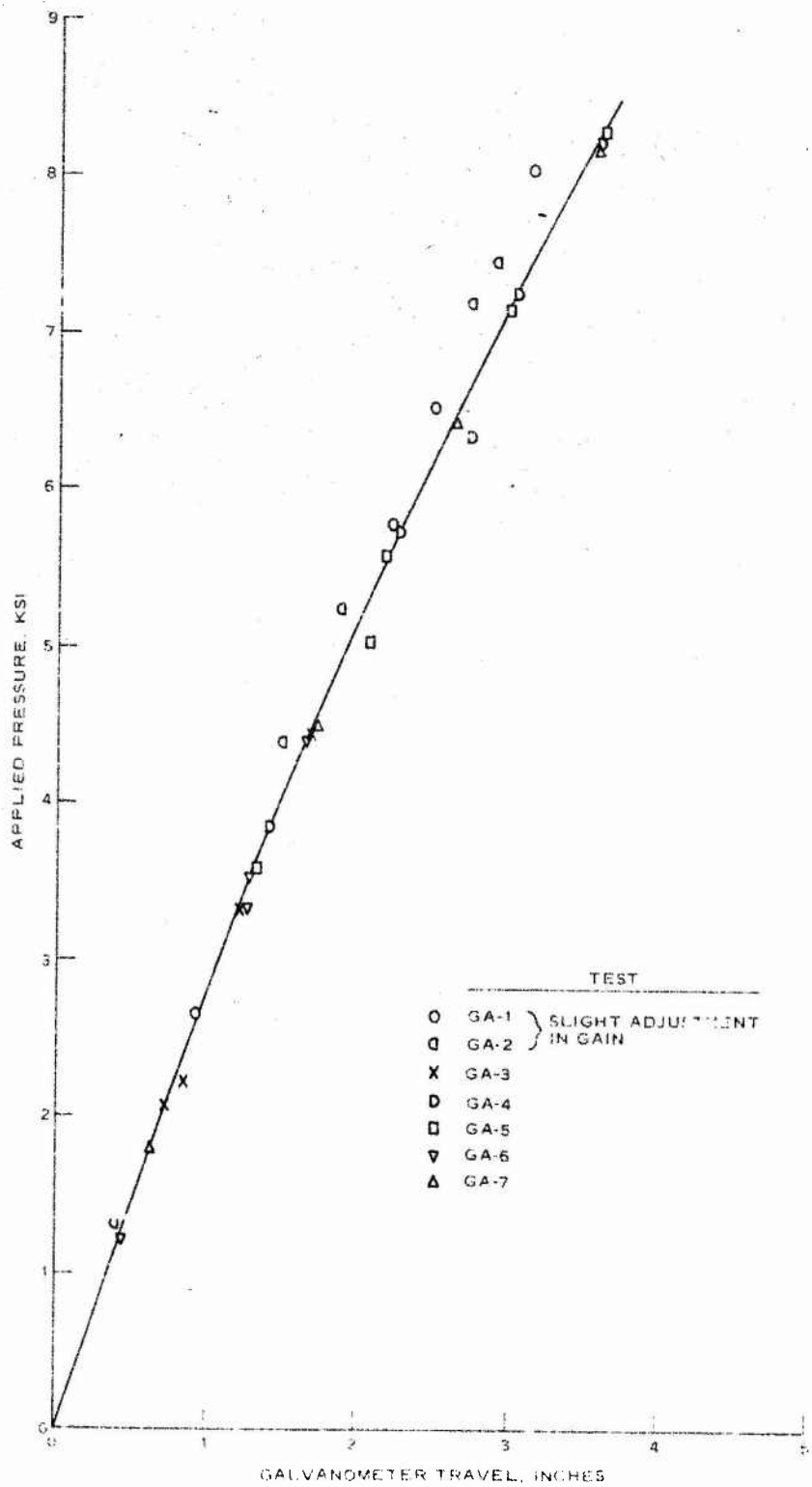

Figure 3.11 Results of seven dynamic calibration tests conducted on GRT Gage No. 1.

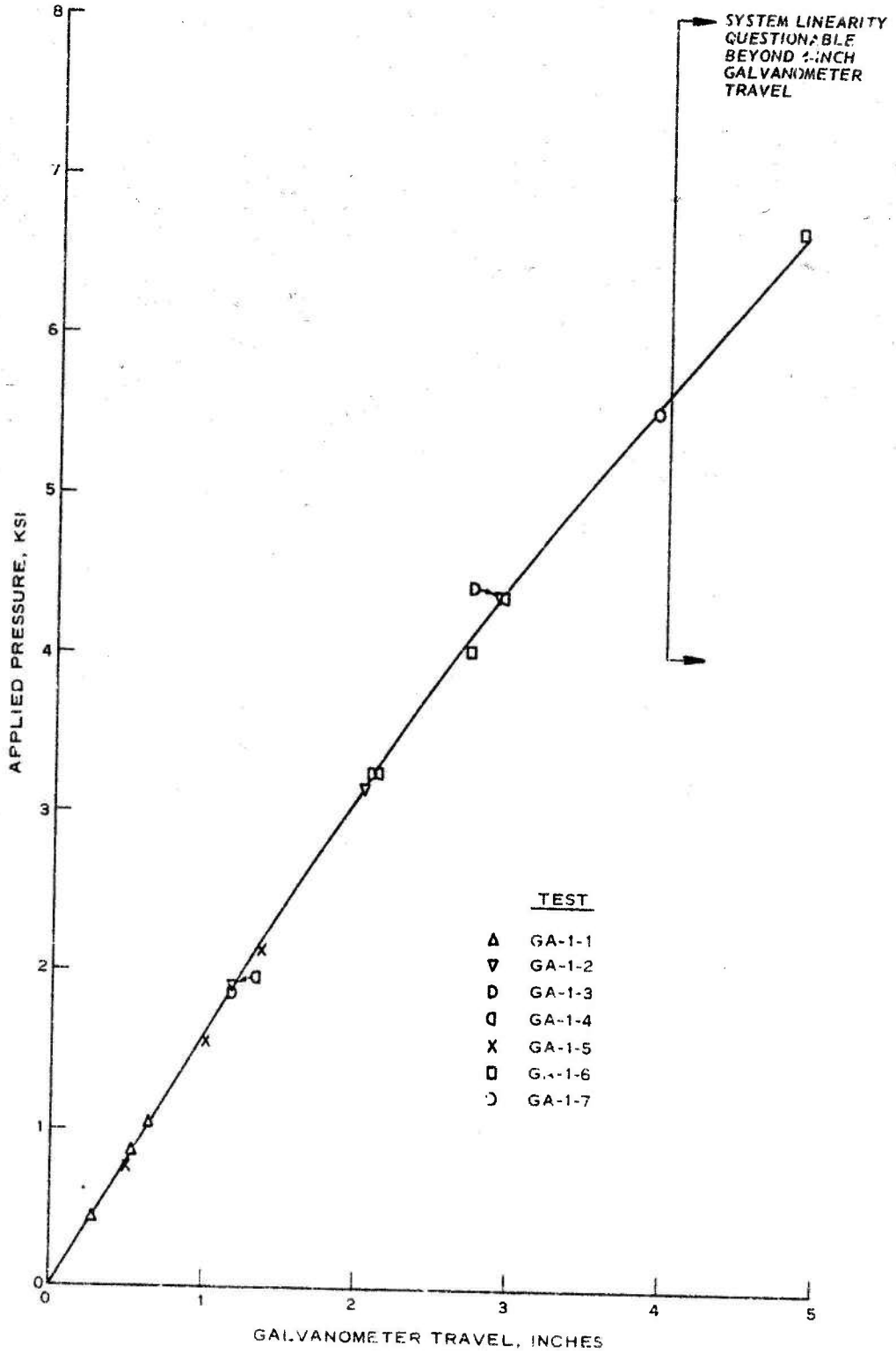

Figure 3.12 Results of sever. dynamic calibration tests conducted on CRT Gage No. 3.

CHAPTER 4

SECOND TEST SERIES: TESTS ON EMBEDDED GAGE

The second main series of tests was conducted with the individual GRT gages embedded in a rock-matching DF5A grout. A grout specimen containing Gage No. 1 was constructed and tested. Later, a second grout specimen containing Gage No. 3 was constructed and tested. The same techniques were used for the construction of both specimens.

4.1 SPECIMEN PREPARATION

A rock-matching grout, DF5A-CS1(1.39), used in some previous NTS events was selected for this study. A brief discussion of the properties of the grout is presented in Appendix A of this report.

Once the gage had been calibrated in oil, it was suspended in a special steel ring approximately 2.5 inches high by 4.8 inches inside diameter and 5.25 inches outside diameter. The steel tubing, which protected the electrical wires connected to the piezoelectric crystal within the gage case, passed through a hole drilled through the side of the ring. The tubing also supported the gage at midheight within the ring. The gage-face centerline was approximately 0.6 inch from the center of the ring due to the length of the steel tubing.

The steel ring containing the gage was placed on a smooth surface and modeling clay was used to seal the bottom of the ring. The DF5A grout was prepared and poured into the ring. The ring was placed in a plastic bag, and a container of water was placed in the bag so the grout could cure in a highly humid environment.

After several hours, the top surface of each specimen was struck off to remove the bleed water which had come to the surface. The plastic bags were then resealed.

Following some period of cure time (17 days for Gage No. 1; 15 days for Gage No. 3), the ring was removed from the bag; the exposed grout surfaces were leveled; and the ring was then placed in the uniaxial strain device. Electrical wires from the gage were extended from the

device and connected to the same recording system used in the calibration of the gage. In general, there were no mechanical or electrical differences between the first and second test series. Preselected pressure pulses were then applied to the grout specimen, and a recording was made of the applied pressure as monitored by the WES pressure transducer and of the output of the grout-embedded gage.

4.2 GRT GAGE NO. 1

A series of seven tests was conducted on GRT Gage No. 1 embedded in the grout specimen with the WES pressure transducer and GRT Gage No. 3 located in the fluid container to measure the applied pressure pulse. The grout specimen was not removed from the device until after the last test. The time between each test was approximately 15 minutes. The results of the seven tests are presented in Figures 4.1 through 4.7. These figures are tracings of the oscillograph records showing the output of the WES pressure transducer and GRT Gages No. 1 and 3. A time scale is shown on each record, and the peak pressure for the WES gage is indicated. The output scale for GRT Gage No. 1 is the same as that used in the first test series; therefore, the oscillograph records from both series, Figures 3.4 through 3.11 and Figures 4.1 through 4.7, may be directly compared. Also, a reference scale factor based on the gage output during the calibration test series for the GRT gage is shown on each record. It should be noted that since the calibration is nonlinear, the scale factor cannot be used as a linear function of galvanometric deflection.

The calibration curves of pressure versus galvanometer travel previously presented in Figures 3.11 and 3.12 are again shown in Figure 4.8. These curves were used in the data reduction of the test results. The following tabulation lists selected data points of applied pressure and pressure measured by the embedded gage for each of the tests:

Test	Applied Pressure	Pressure Measured by GRT Gage No. 1
	psi	psi
GA-1-1	446	225
	863	290
	1,022 (peak)	325
GA-1-2	1,904	375
	3,180	475
	4,374 (peak)	2,250
GA-1-3	1,883	400
	3,273	2,425
	4,334 (peak)	3,675
GA-1-4	1,873	700
	3,273	2,250
	4,374 (peak)	3,725
GA-1-5	844	450
	1,638	1,175
	2,143 (peak)	1,675
GA-1-6	6,668 (peak)	5,850
	4,043	3,750
GA-1-7	9,757 (peak)	7,700
	5,537	5,150

In the first test shown in Figure 4.9 the peak applied pressure is approximately 1,000 psi; however, the embedded gage's (Gage No. 1) output indicates only 325 psi. Note that only a few data points are plotted to indicate the trend of the test results. In the second loading shown in Figure 4.9 the applied pressure is approximately 4,400 psi, but the output from Gage No. 1 indicates only approximately 2,200 psi. The 4,400-psi pulse was repeated in the third and fourth tests. Gage No. 1 did not respond properly to the rise portion of the pulse in the third and fourth tests shown in Figure 4.9; however, thereafter the gage did register closer to the applied pressure. The fifth test was conducted at a lower peak pressure, 2,200 psi, and the pressure registered by the embedded gage was slightly lower than the applied pressure. The rise time of the pulses in the last two tests shown in Figure 4.9, 6 and 7, was changed to 3 msec. The approximate peak pressures were

6,700 psi and 9,800 psi for tests 6 and 7, respectively, and the gage successfully followed the applied pulse oscillations but registered slightly low in pressure. The peak pressure of test 7 was 9,800 psi, and the gage measured only 7,700 psi; however, this large a discrepancy could not have been due to electrical and resolution limitations.

After the last test, the uniaxial strain test device was disassembled, and the grout specimen containing Gage No. 1 was removed. A small quantity of free water was noted around the grout specimen. Since the specimen was separated by a membrane from the oil-filled fluid container, the water found around the specimen must have been squeezed out of the grout material during the test series. It is not known when during the seven tests that the water was forced out.

4.3 GRT GAGE NO. 3

A second grout specimen containing Gage No. 3 was also constructed. The cure time for this specimen, as noted in Appendix A, was 15 days. One test was performed on embedded Gage No. 3, and the oscillograph record from that test is shown in Figure 4.10. A peak pressure of 4,300 psi was applied with a rise time of 4 msec. The following tabulation lists some of the data points obtained from the oscillograph record:

Test	Applied Pressure	Pressure Measured by GRT Gage No. 3
	psi	psi
GA-2-1	1,205	550
	3,012	2,000
	4,117	4,525
	4,297 (peak)	4,675

The gage responded satisfactorily to the applied pressure, except during the initial rise portion of the applied pulse. Figure 4.11 shows the pressure measured by Gage No. 3 versus applied pressure during the rise portion and during a part of the decay portion of the test. After

the test, when the device was disassembled, some water was found around the specimen. It is believed the free water was forced out of the grout during the test.

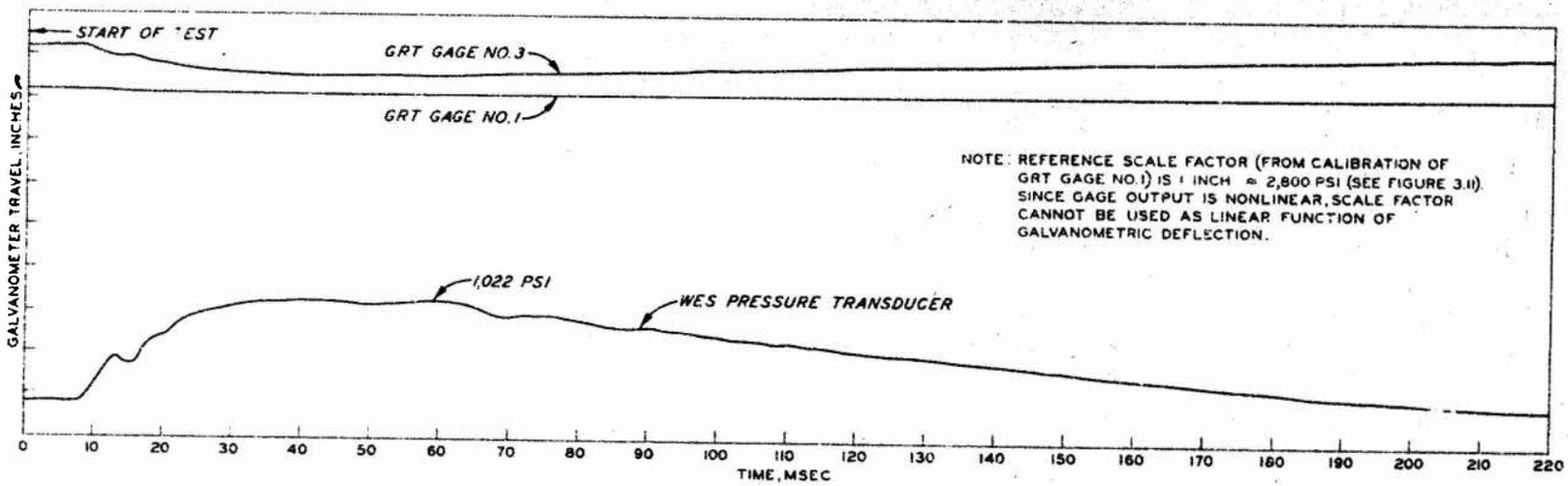

Figure 4.1 Tracing of oscillograph record from Test GA-1-1.

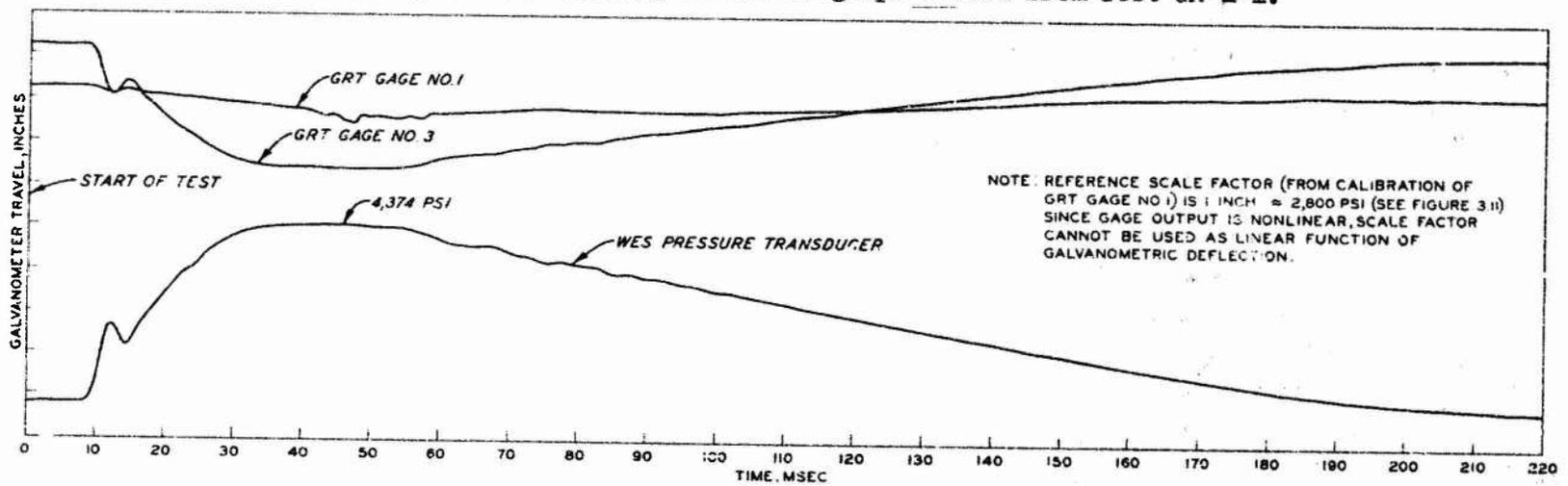

Figure 4.2 Tracing of oscillograph record from Test GA-1-2.

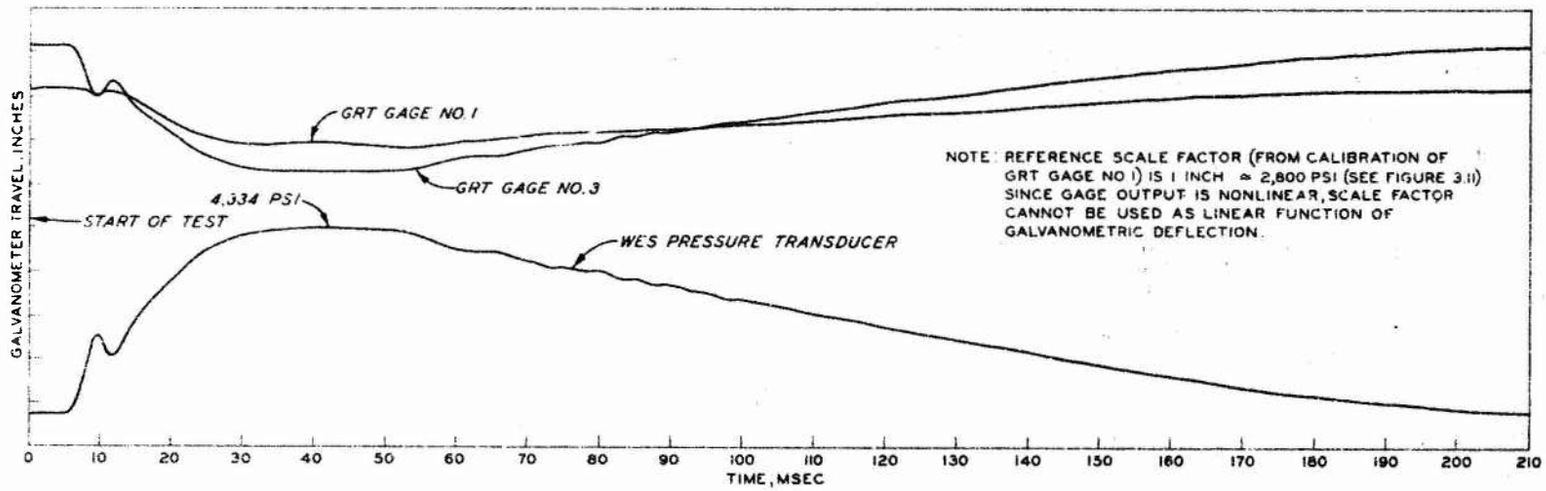

Figure 4.3 Tracing of oscillograph record from Test GA-1-3.

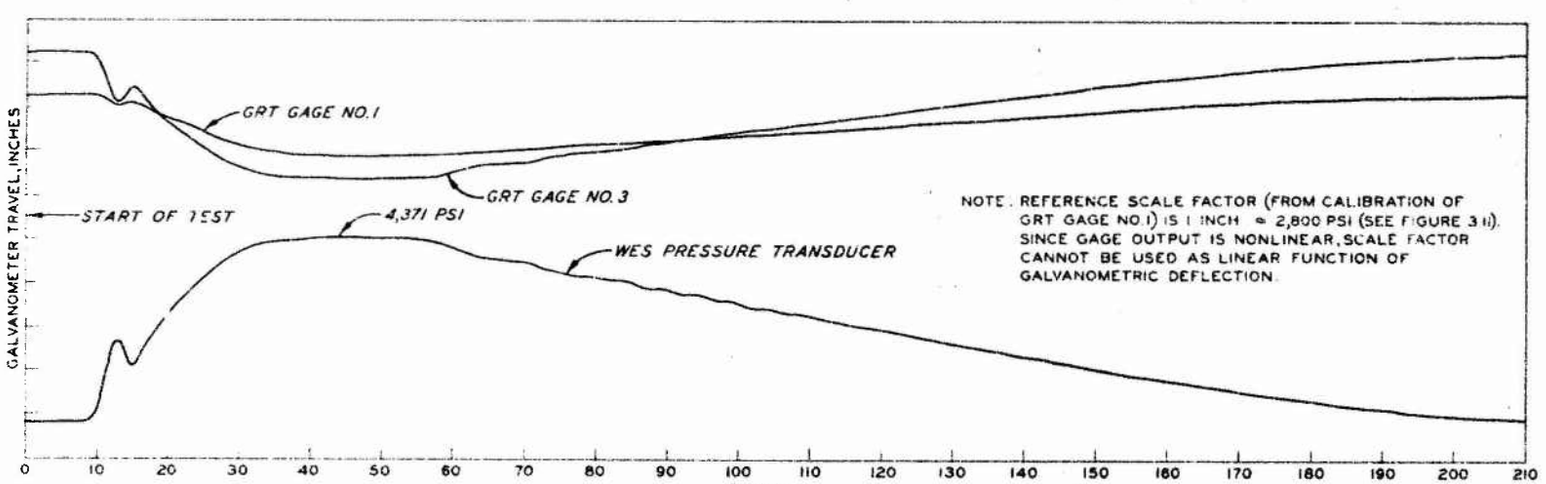

Figure 4.4 Tracing of oscillograph record from Test GA-1-4.

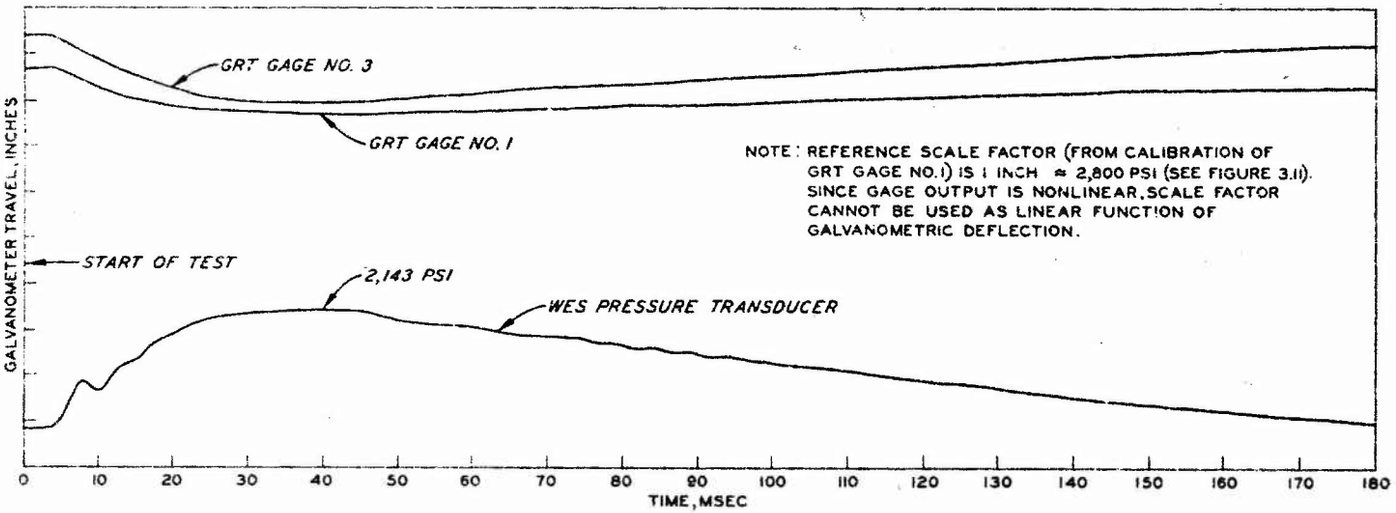

Figure 4.5 Tracing of oscillograph record from Test GA-1-5.

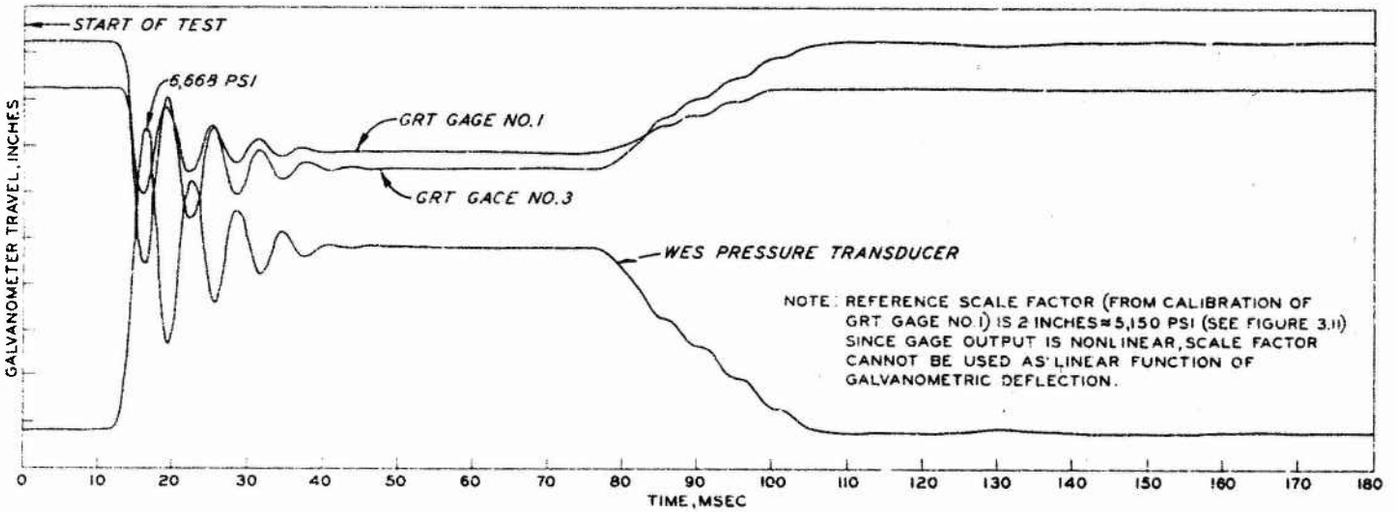

Figure 4.6 Tracing of oscillograph record from Test GA-1-6.

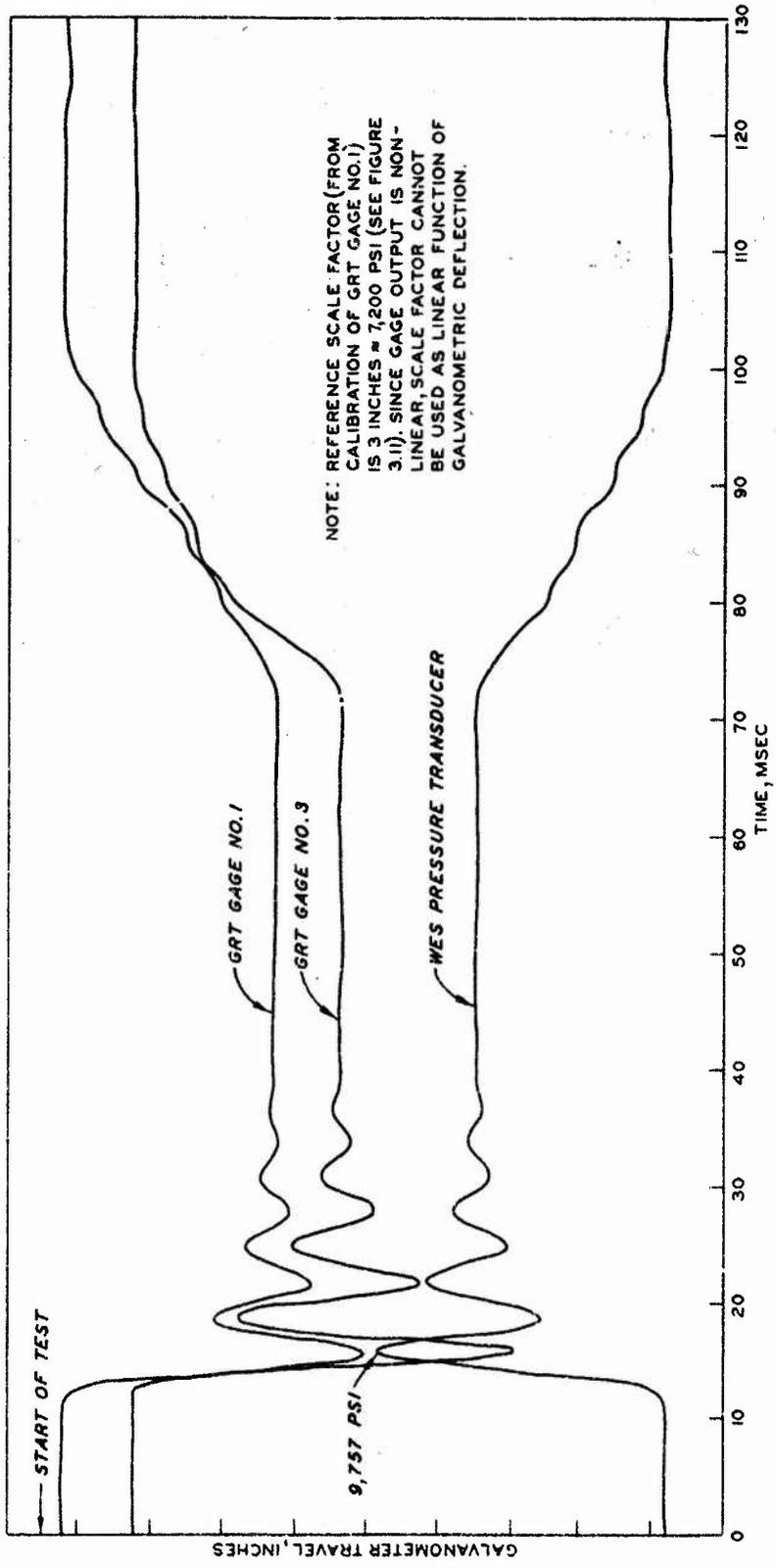

Figure 4.7 Tracing of oscillograph record from Test GA-1-7.

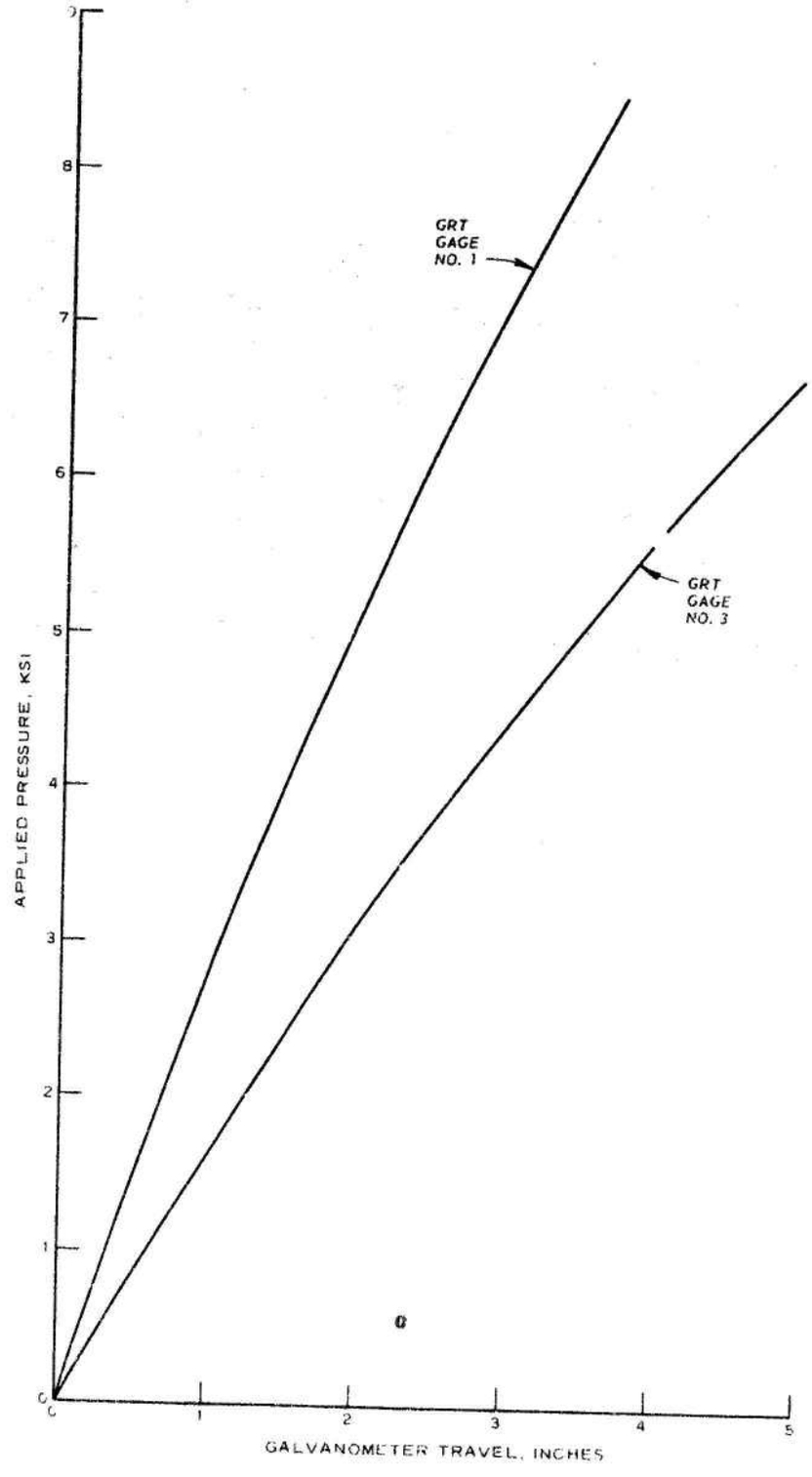

Figure 4.8 Calibration curves of GRT Gages No. 1 and 3.

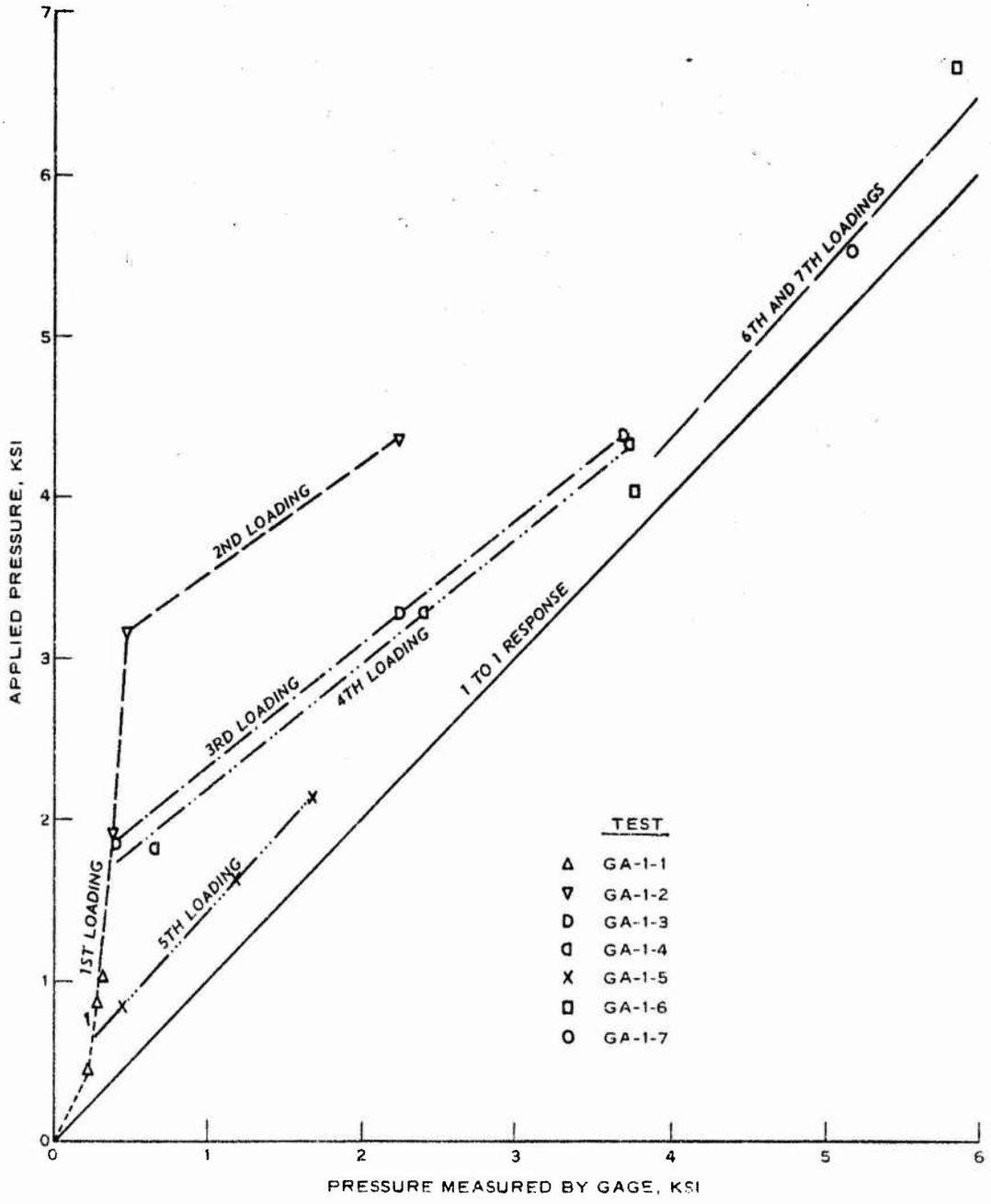

Figure 4.9 Results of seven dynamic tests conducted on GRT Gage No. 1 embedded in grout.

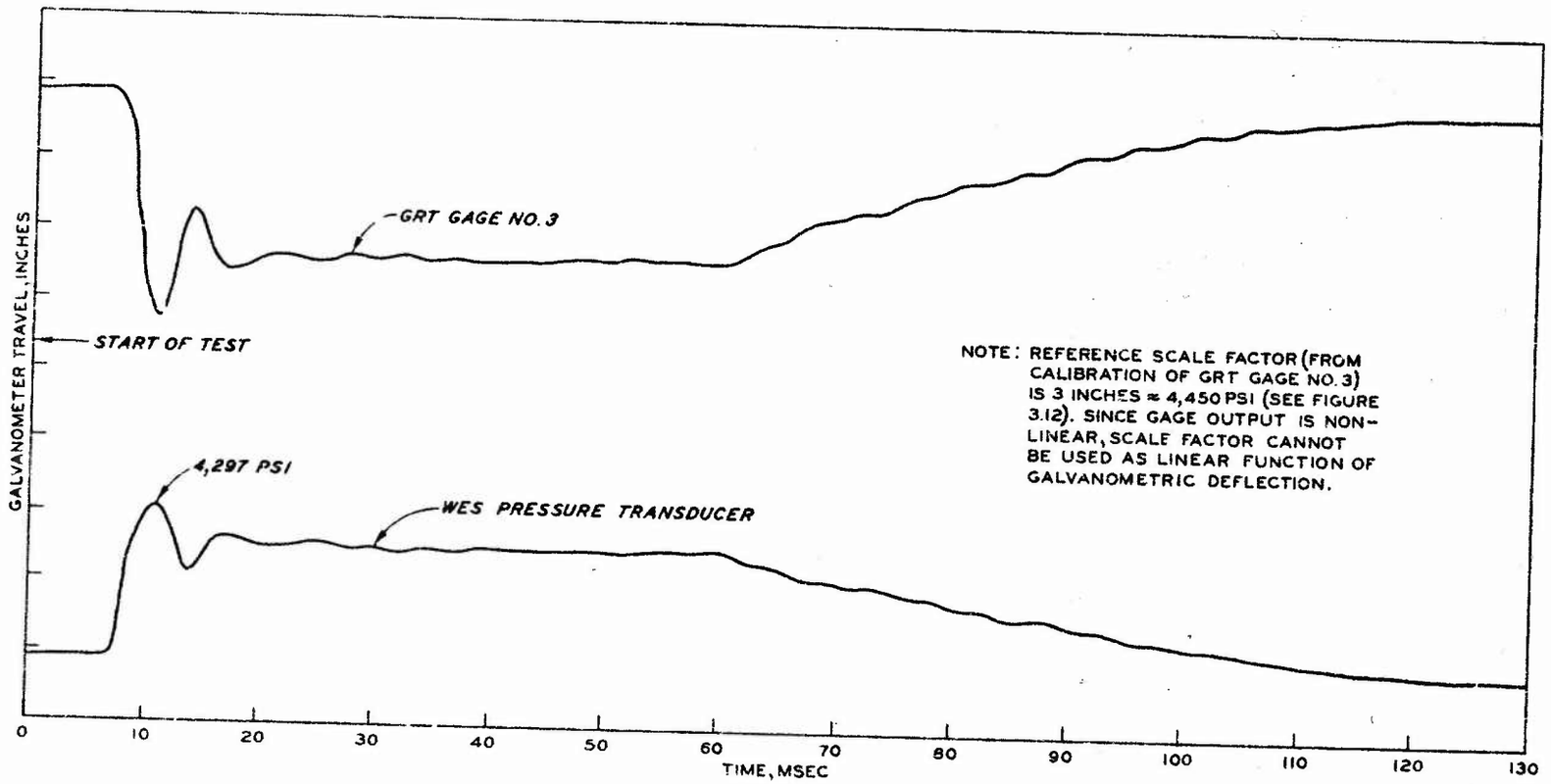

Figure 4.10 Tracing of oscillograph record from Test GA-2-1.

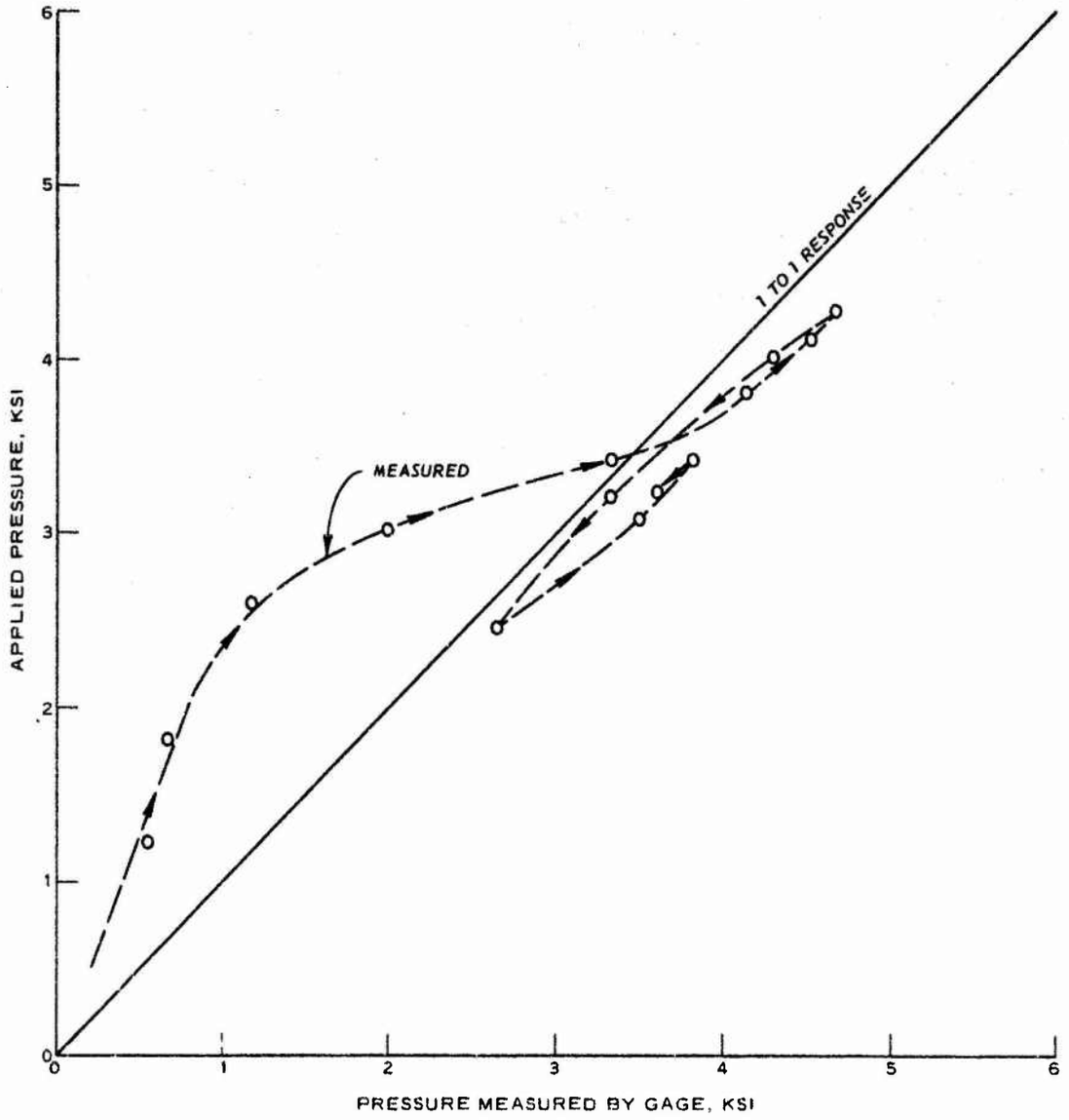

Figure 4.11 Results of one dynamic test conducted on GRT Gage No. 3 embedded in grout.

CHAPTER 5

DISCUSSION OF TEST RESULTS

5.1 CALIBRATION TESTS

The results of the calibration series on the gages showed that a nonlinearity exists in the output of the gages. The gage output appears to agree with GRT calibration data at the low pressure range (up to 3,000 psi), but, at higher pressures (up to 8,000 psi), the output of the gage is greater than that predicted by extrapolation of the low-pressure-range calibration. Because the output beyond 8,000 psi was not investigated, it is not known if the output continues to become more nonlinear in fashion or if the output from 3,000 to 8,000 psi can be extrapolated to higher pressures.

5.2 TESTS ON EMBEDDED GAGES

The results of the tests on the gage embedded in grout indicate that the gage output can be influenced by surrounding media. The first two tests on GRT Gage No. 1 indicated that the gage only measured 25 to 50 percent of the applied pulse. By the third test, the gage began to respond more closely to the applied pulse; in the last three tests, the gage response was much more consistent. The results of the one test on GRT Gage No. 3 indicated that the gage overregistered the applied pressure by 10 percent, except during the initial portion. In both test series, free water was found around the grout specimen when the device was disassembled.

5.3 POSSIBLE EXPLANATIONS OF TEST RESULTS

There are several possible explanations for the above results. First of all, the boundary conditions of the test specimen could affect the stress distribution within the specimen due to sidewall friction. However, an investigation of granular and cohesive materials (Reference 1) has shown this effect to be minimal. Since the gages were nearly centered within the specimens, it is not believed that

boundary conditions can explain the large discrepancies seen in the first test results. Also, the results of the analytical investigation using a finite element computer code (see Appendix B) indicate that the axial stress distribution within the center portion of the specimen is unaffected by sidewall friction. Although simplified assumptions were made, the calculations did consider the grout welded to the steel ring and did represent an extreme condition.

Secondly, a rigid gage in the grout material could cause a nonuniform stress distribution within the specimen. The results of the calculations (Appendix B) indicate a stress concentration at the edge of the gage and a high axial stress distribution directly over the gage. The gage might therefore overregister by 5 to 10 percent.

Thirdly, an arching effect by the grout across the relatively small gage face (1/2-inch diameter) could have prevented the full transmittal of stresses to the gage. The material may have been initially in contact with the gage, but, when the material was loaded, it transferred the stresses around the gage. This phenomenon could exist when there is a stiffness mismatch between the gage and the earth material.

Finally, a water-filled or an air-filled void between the gage face and surrounding grout material might alter the stress distribution above the gage. The calculations discussed in Appendix B indicate that a water-filled void should not greatly alter the axial stress distribution, based on those material properties assumed for grout and not allowing for flow of the water out of the void.

The results of uniaxial strain tests on the grout presented in Appendix A disclose the apparent ability of the grout material to expel water even under dynamic loading rates. These results may indicate that pore water can flow into or out of any void within the specimen. If water can flow out of a void existing above the gage, then it may be possible for a lower axial stress distribution over the gage to develop than is indicated by the calculations in Appendix B, due to relief of the water pressure.

The calculations show that an air-filled void could severely reduce the axial stress applied to the gage face, resulting in underregistration

of the gage. The calculations also imply that a void under the gage should have also reduced the axial stress on top of the gage. Subsequent collapse of the void, due to grout structure breakdown, might then allow the material to transmit the applied stress to the gage. Although it is not known how an air void across the gage face could have been created, even a slight separation between the gage and grout would prevent the full transmittal of stresses. A possible explanation of how air could be trapped under the gage is that, during the first few hours after the grout preparation, the bleed water that rose to the top of the specimen could have carried some trapped air with it. Some of the air and water could have been trapped under the gage during that period of time creating a slight void.

CHAPTER 6

CONCLUSIONS AND RECOMMENDATIONS

The purpose of this study was to determine if a stress gage's output is affected by embedment in a grout. Two stress gages furnished by GRT were calibrated in a fluid environment under a variety of pressure pulses. The gages were then embedded in wafer-shaped specimens of a rock-matching grout, DF5A. The grout specimens containing the gages were subjected to a series of measured pressure pulses, similar to those pulses used in the calibration test series. Uniaxial strain tests were also conducted on separate grout specimens. An analytical investigation using a finite element computer code was also conducted to determine if some insight could be gained into the gage response.

6.1 CONCLUSIONS

The GRT gage has a slightly nonlinear calibration curve when calibrated in oil. If the gage is to be used at pressures greater than 8,000 psi, calibration tests at higher pressures should be conducted.

Pressures measured with a stress gage embedded in a uniaxial strain specimen of grout do not always correspond closely to pressures measured in the oil on the surface of the specimen only 1-1/4 inches from the gage face. The cause of the difference is believed to be related to the inhomogeneities in the material resulting from placement and the way they influence material-gage interaction and not to the electrical or mechanical operation of the GRT gage itself.

The material surrounding an embedded stress gage in grout could greatly influence the response of the gage.

Although the experimental and analytical investigations were limited, it appears that gage-placement technique, for a well-designed gage such as this one, is the single most important controlling factor in influencing gage response.

6.2 RECOMMENDATIONS

The results of this study indicate the need for a controlled parameter study, both experimental and analytical, of those factors thought to influence the gage response. For example, grout specimens with embedded gages could be prepared with known air- and water-filled voids above the gage face. The analytical portion of the study would then model the known test conditions to determine if the experimental results were predictable. The finite element computer code could be modified to incorporate slip elements and appropriate properties of the piezoelectric crystal located at the center portion of the gage to reduce gage stiffness.

The results of the controlled parameter study could then be used in developing gage-placement techniques to ensure optimum gage response within the embedded material. It is realized that an important factor in the measurement of free-field ground shock is the transfer of the stress pulse propagating through the natural, in situ earth material to the material containing the embedded stress gage. However, placement techniques must first be developed which ensure proper gage response within just the embedded material.

APPENDIX A

UNIAXIAL STRAIN TESTS ON GROUT

At the outset of this study, it was recognized that some stress-strain data for the grout used in the stress gage tests would probably be needed in the interpretation of the response of the embedded stress gages and that there was a lack of information on the constitutive properties of the rock-matching grout used at NTS in a state of uniaxial strain. Therefore, during the preparation of the special grout specimens used in this study, additional grout specimens of the size needed for uniaxial strain tests were prepared. These specimens were prepared at the same time as the specimens used for the gage evaluation and were made from the same two DF5A batches[1] used for the gage evaluation specimens. These specimens were then tested in the uniaxial strain device after approximately the same cure time as had been applied in the gage evaluation tests. Measurements of the applied axial stress and axial deflection were made. These data were used to construct a plot of axial stress versus axial engineering strain for each test. The slope of a curve of this type is by definition the constrained modulus M.

A.1 MATERIAL DESCRIPTION

The grout used in this study was DF5A-CS1(1.39), a slightly expansive rock-matching grout. The color of the grout varied; the first batch was tan, and the second batch was gray. The difference in color was probably due to differences in the color of the barite used in the mix. The following tabulation presents some of the physical properties determined from previously tested grout of this same type.[2]

---

[1] Specimens prepared by Grouting Section, Concrete Laboratory, WES.

[2] Information supplied by Grouting Section, Concrete Laboratory, WES.

Cure Time	Unconfined Compressive Strength	Compressional Wave Velocity
days	psi	ft/sec
7	860	--
34	1,360	7,245
44	1,440	7,655

The percentage of water used in the grout mix was 36.2 percent by weight of water to dry solid weight or 26.6 percent by weight of water to weight of total material. Approximately 30 percent of this water is used up in the hydration process (Reference 2). The grout has a design wet density of 127 pcf. The design air value is 5 percent of the total volume.

A.2 UNIAXIAL STRAIN TEST PROGRAM

One static (2 minutes to peak stress) and two dynamic (approximately 25 msec to peak stress) uniaxial strain tests were performed on specimens whose dimensions were 5 inches in diameter by 2-1/2 inches high. The average wet density of the three specimens was 132 pcf. The axial stress versus axial strain curve for the first test (a static test with approximately 2 minutes to peak pressure), which was conducted on a specimen with a cure time of 15 days, is shown in Figure A.1. When the test device was disassembled after the test, free water was noted around the specimen.

The second and third tests were conducted on specimens after 16 and 20 days cure time, respectively. The axial stress versus axial strain and the axial stress versus time curves for each test are shown in Figures A.2 and A.3. The axial stress was applied to the specimen with the 16-day cure in 35 msec (rise time) followed by a 60-msec decay. No free water was noted around the specimen at the end of the test. The test on the specimen with a 20-day cure, shown in Figure A.3, had a 25-msec pressure rise time, a 15-msec hold time, and a 70-msec decay. After the test, free water was noted around the specimen.

Only one test was conducted on the second batch of DF5A grout. The results from this test, which had a 25-msec rise time and a 50-msec decay time, are shown in Figure A.4 as plots of axial stress versus axial strain and axial stress versus time. The cure time of the grout was 13 days. The water content (obtained from trimmings) and the compressional wave velocity were measured on this specimen prior to the uniaxial strain test. These data are listed in Figure A.4. Free water was found around the specimen after the test.

A.3 DISCUSSION OF TEST RESULTS

Only one test was conducted on the grout in which drainage was either prevented or so slight that posttest free water could not be observed. This is the test shown in Figure A.2. The secant constrained modulus to an axial stress of 6 ksi for this dynamic test on the grout with a 16-day cure time was 45×10^4 psi. Above 6 ksi, the material began to increase in stiffness, as shown in Figure A.2.

The remaining tests on the grout specimens all experienced drainage during the load cycles. It is believed that the softening of the stress-strain curve, as seen in the test results shown in Figures A.1, A.3, and A.4, could be the result of loss of water from each specimen during its testing. Such drainage would result in a corresponding additional volume decrease of the material during loading. It also could be associated with a structural collapse of the cement matrix with enclosed air voids.

It is not understood why the one dynamic specimen tested after 16 days of cure did not drain, whereas the specimen tested after 20 days did drain. The specimens were prepared from the same batch of grout and were cured and tested in the same manner.

The tests in which drainage occurred may not be valid for approximating field conditions. In the field, with the exception of local voids and fractures such as those due to blasting during tunnel advance, there are probably few drainage paths around the grout mass into which the water can escape. However, if these local voids are of significant number or size, it may be possible for the water to migrate into them

and the response of the material might then be similar to that of the drained test results. The significant point indicated by these data is that the grout can drain under rapid loading provided there are sufficient drainage paths.

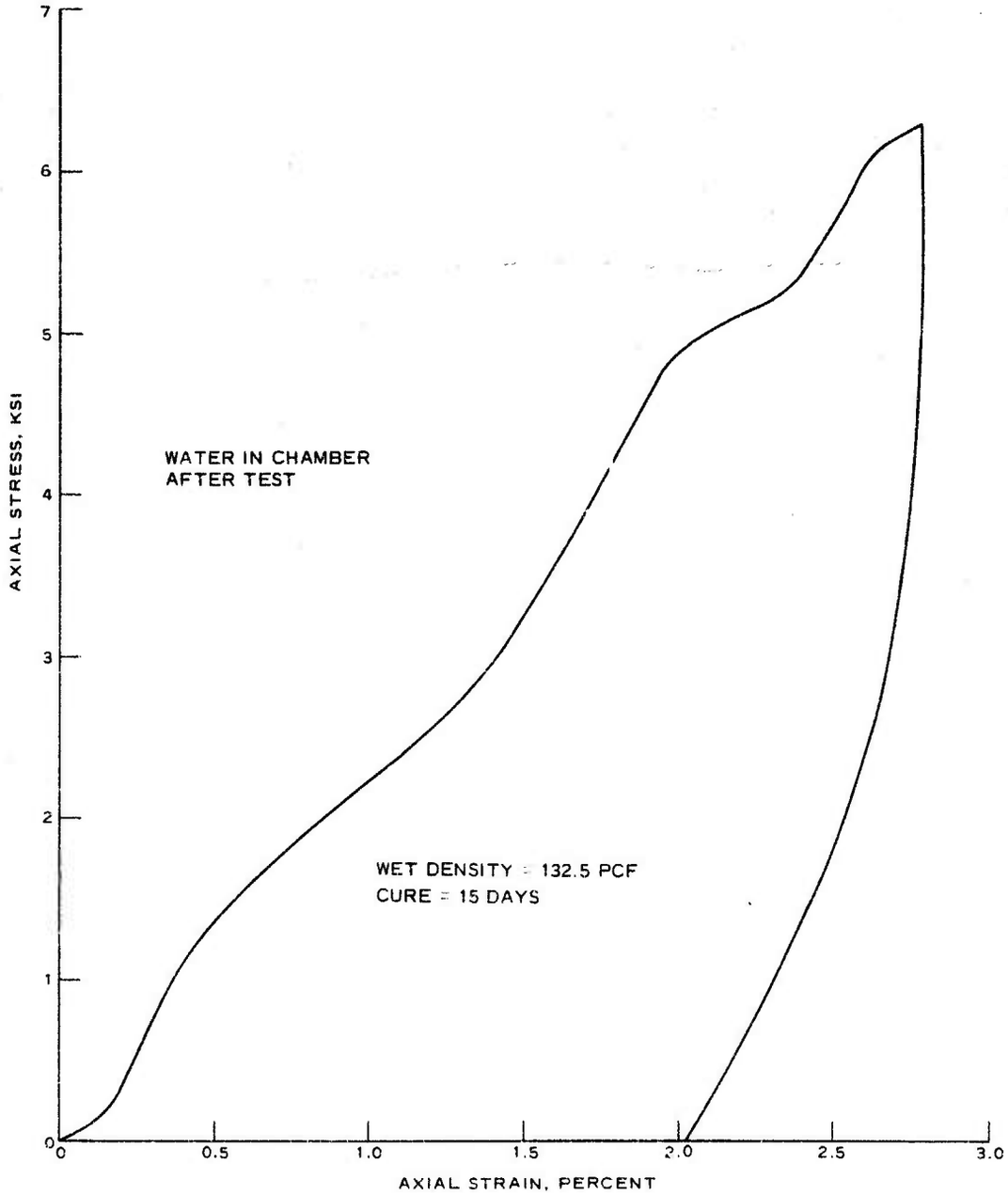

Figure A.1 Uniaxial strain test results on grout, 15-day cure time.

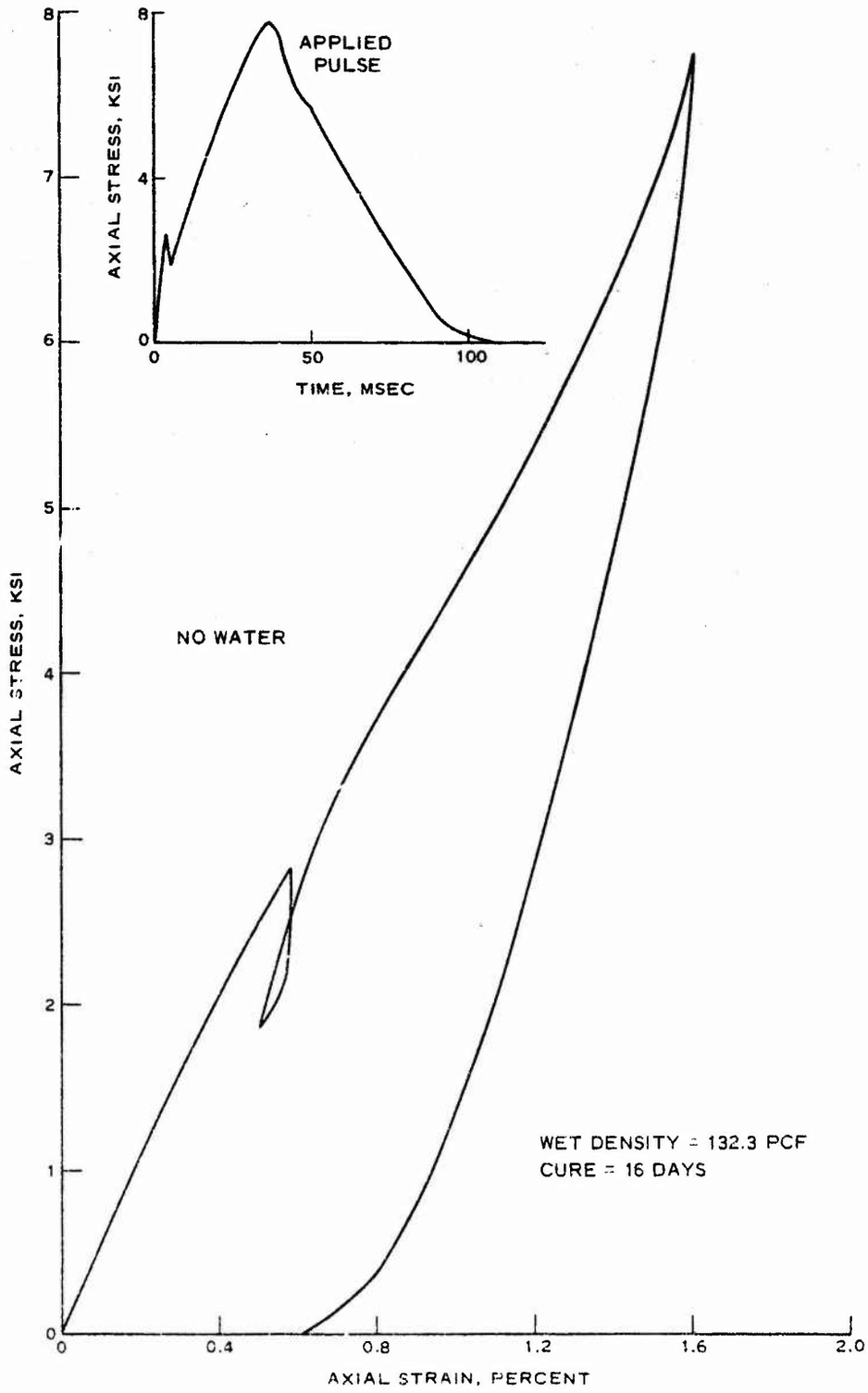

Figure A.2 Uniaxial strain test results on grout, 16-day cure time.

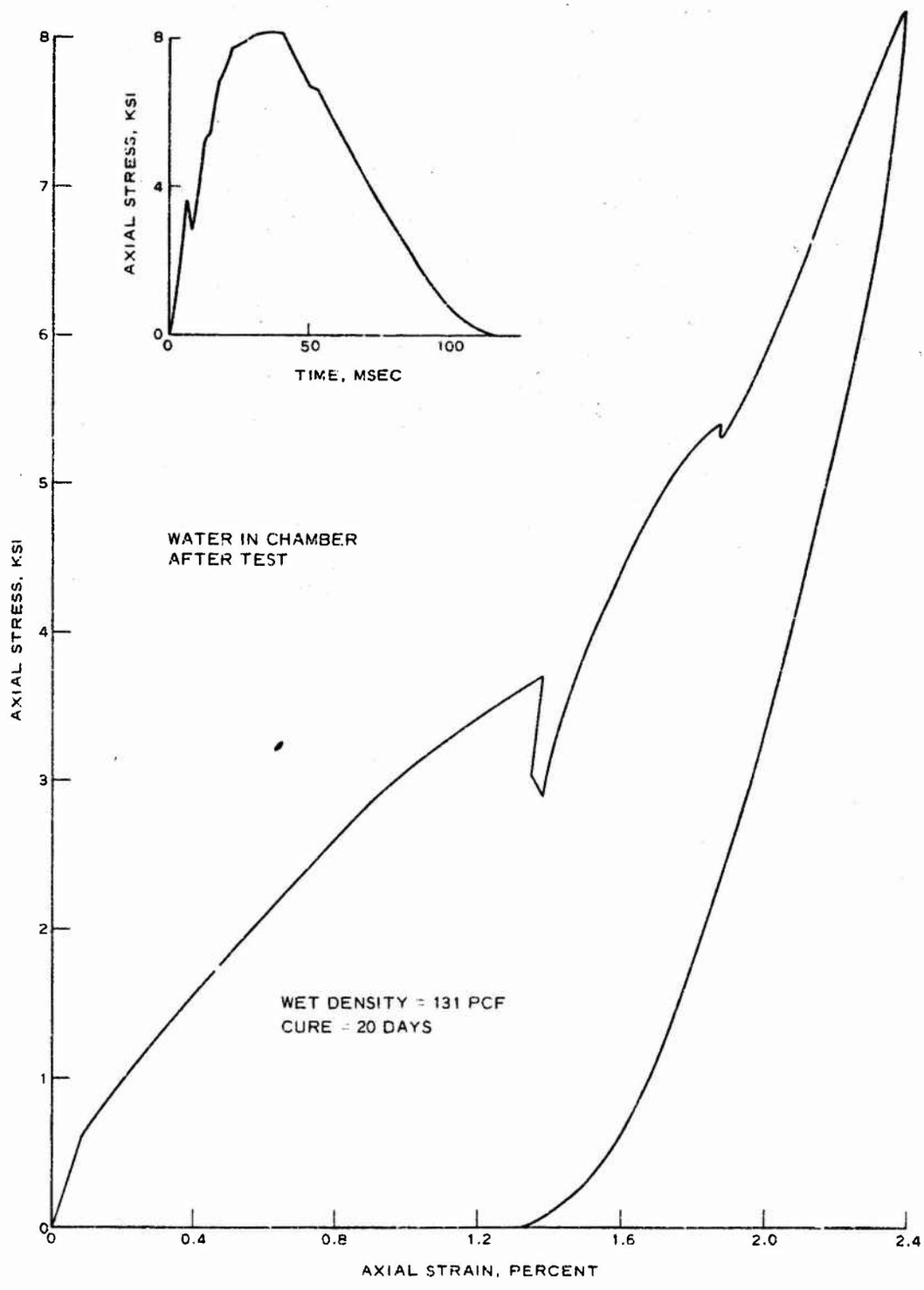

Figure A.3 Uniaxial strain test results on grout, 20-day cure time.

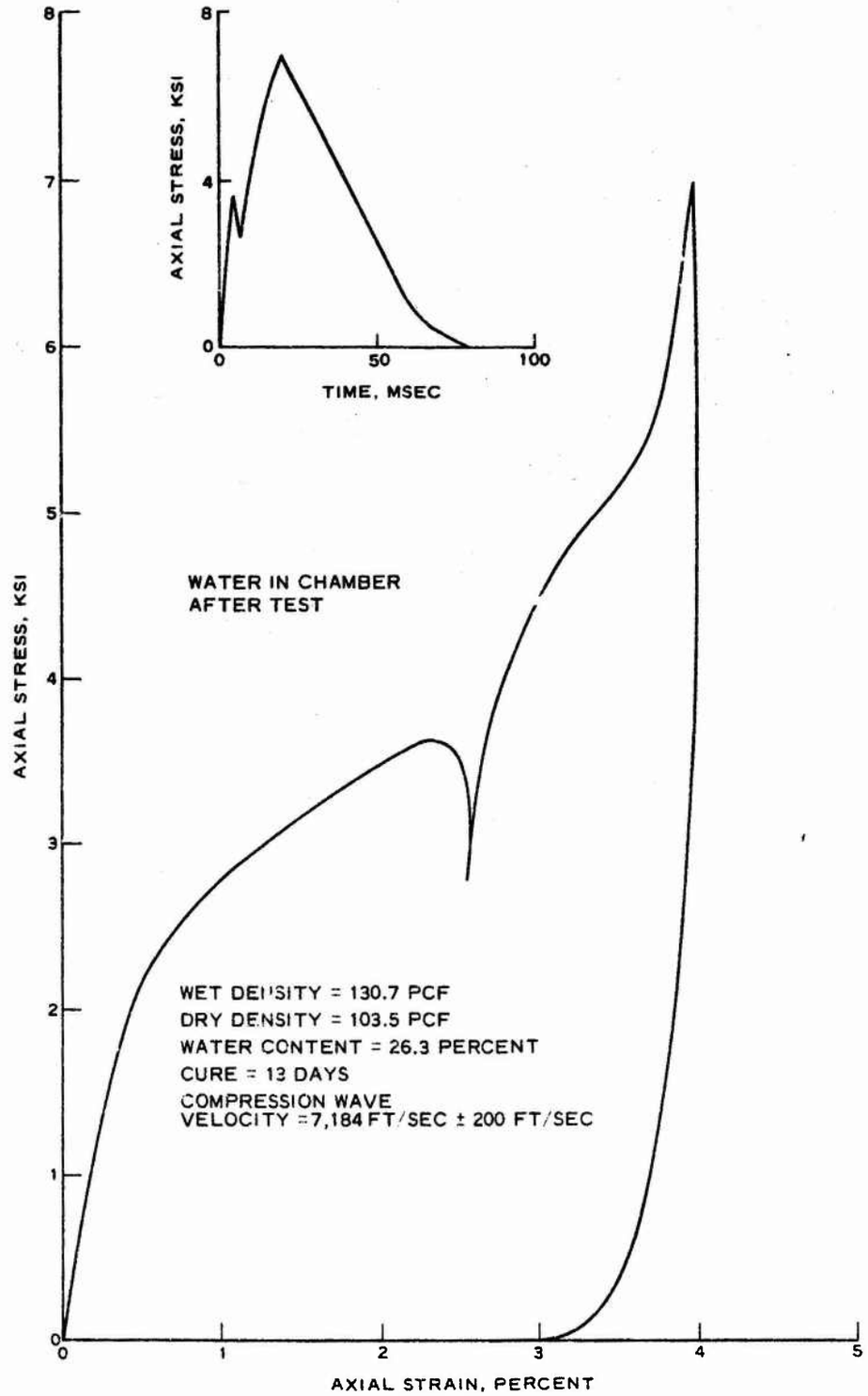

Figure A.4 Uniaxial strain test results on grout, 13-day cure time.

APPENDIX B

ANALYTICAL STUDY OF FACTORS THAT INFLUENCE GAGE RESPONSE

B.1 BACKGROUND

A series of dynamic uniaxial strain tests was conducted on two grout specimens, each containing a stress gage developed by GRT. In the first part of these tests, seven successive dynamic pulses of various stress levels and pulse durations were applied to a grout specimen containing a GRT gage. The GRT gage underregistered the applied stress by 50 percent during the first two tests. The gage response improved thereafter and became more consistent. The gage did, however, continue to register a lower pressure than was applied. In the second part of the series, one dynamic test was conducted on another grout specimen containing a GRT gage. As the pressure was applied, the gage at first underregistered the pressure, but, at approximately peak applied pressure, the gage was overregistering by 10 percent of the applied pressure.

Several possible explanations for the test results put forward as hypotheses are as follows: (1) the grout specimen (approximately 4.8-inch diameter by 2-1/2-inch height) was prepared and tested in a steel ring, and sidewall friction developed during loading and prevented the full applied stress from reaching the gage, (2) the steel-cased gage was less compressible than the surrounding grout; therefore, the stress distribution in the grout was altered in the area of the gage, causing the overregistration in the one case it was observed, or (3) a void, either empty or partially filled with water, which was located directly over the gage face, prevented the full applied stress at the surface of the grout from reaching the gage in the cases in which underregistration was noted.

B.2 PURPOSE

The purpose of this investigation was to determine analytically, with the use of a nonlinear finite element computer code, WESTES, if any

of the above-mentioned explanations of the experimental test results could be verified.

B.3 SCOPE

Four different code calculations were performed for loadings of the following: (1) the steel ring and grout, (2) the ring, grout, and gage, (3) the ring, grout, gage, and a water-filled, 20-mil-thick void above the gage, and (4) the ring, grout, gage, and an air-filled, 20-mil void above the gage. Ten loading increments of 400 psi each were simulated on the top of the grout specimen. This appendix presents the calculated results of the axial stress within selected elements of the specimen for the peak applied surface pressure of 4,000 psi. The axial stress distribution across the grout specimen at the elevation of the gage is discussed for each of the four cases.

B.4 DESCRIPTION OF STUDY

An analytical investigation using a previously developed axisymmetric finite element computer code, WESTES (Reference 2), was conducted using boundary conditions and material properties believed representative of the grout specimen and gage. Figure B.1 shows a cross section of the steel ring, grout specimen, and embedded GRT stress gage as they were tested. Note that the tube attached to the gage, which protected the lead wires, prevented placement of the gage directly in the center of the specimen. Figure B.2 shows a half section of the ring, grout, and gage as they were idealized for the finite element code calculation. The gage was idealized to be at the center of the specimen for reasons of symmetry and therefore reduced a general three-dimensional problem to an axisymmetric problem. The half section was divided into four zones: Zone 1 represented the steel ring, Zone 2 represented the grout material, and Zones 3 and 4 allowed representation of the gage and a 20-mil void above the gage, respectively. The table in Figure B.2 lists the four cases studied in the investigation to determine if: (1) the sidewall friction between the grout and steel ring affected the gage, Case I, (2) a rigid gage in the grout altered the stress distribution,

Case II, (3) a void filled with water above the gage affected the gage output, Case III, and (4) a void filled with air above the gage affected the gage output, Case IV.

B.5 CODE DESCRIPTION

WESTES is an axisymmetric nonlinear finite element code programmed to solve boundary value problems in soil continuum mechanics. The code uses a variable-moduli-type constitutive model (Reference 3) to describe the nonlinear behavior of the material. Constant-strain triangular elements, which are internally developed from input quadrilateral elements, are used, and the nonlinear problem is solved in an incremental manner. Each increment is solved in two steps to increase the accuracy of the solutions. The code can handle loading, unloading, and reloading. If the material yields, the code sets the shear modulus to a small value and adjusts the deviatoric components of the stresses to satisfy the yield criterion. The code prints out the components of stresses and strains in each element and the components of displacements at all the nodal points.

In the finite element idealization of the problems under consideration, the contact planes between the steel and grout and the gage and grout were assumed to allow no relative slippage between the materials. In other words, the grout was assumed to be glued to the steel and the gage. No slip elements were used in the analysis, because they are not available within the capability of this code.

The continuum was divided into 405 elements and 423 nodal points. A larger number of smaller elements were used in zones where stress concentrations were expected. The nonlinear problem was solved using 10 increments of loading. A uniform loading increment was applied across the top surface of the grout and ring.

B.6 MATERIAL PROPERTIES

The input material properties of the steel ring were: (1) bulk modulus $K = 25 \times 10^3$ ksi linear and (2) shear modulus $G = 11.5 \times 10^3$ ksi linear.

The input material properties of the grout included a linear bulk modulus K and a shear modulus G, which is a function of only the square root of the second invariant of deviator stress $\sqrt{J_2'}$ and is independent of the mean normal stress p. The yield strength was 0.8 ksi at all levels of p. The values of K and G were taken as

$$K = 300 \text{ ksi linear}$$

and

$$G = 180 \text{ to } 225 \sqrt{J_2'}$$

$$G = 0.1 \text{ ksi after yielding}$$

The grout properties were estimated using the test results presented in Appendix A and the assumptions that (1) the initial value of Poisson's ratio is 0.25, (2) the yield envelope is flat, or (3) peak deviator stress does not increase with p, and G varies linearly with $\sqrt{J_2'}$. The input material properties of the water were $K = 300$ ksi and $G = 0.01$ ksi.[1] The input material properties of air were $K = 0.01$ ksi and $G = 0.01$ ksi.[1]

B.7. AXIAL STRESS DISTRIBUTION WITHIN THE GROUT SPECIMEN

In the first case, Case I, only the steel ring and grout were considered, and the axial stress distribution within the specimen was determined. The elements of grout were considered glued to the steel elements in the finite element calculations. This case is thought to be the most severe condition for wall friction since no slippage is allowed. Figure B.3 shows a half section of the specimen and the grid locations of four layers of elements. It should be noted that, because of the scale selected for Figure B.3, the last four groups of elements in Layer No. 2 (on the right side) represent two or three elements each. The numbers shown in each element were the element numbers used in the calculation.

Figure B.4 is a plot of the axial stress in each of the elements across the four layers shown in Figure B.3 for an applied stress of

---

[1] $G = 0$ is not permitted in the code.

4,000 psi to the surface of the grout. The plot indicates that the effect of the steel boundary was to decrease the magnitude of axial stress within the grout near the ring. The influence of the boundary appears to increase with depth; however, the center portion of the specimen appears unaffected by the ring. It is thought that, if slippage between the grout and ring was allowed, the effect of sidewall friction would not extend as far from the ring within any given layer as is shown here. Figure B.5 shows a half section of the specimen and the locations of the elements in the four layers where the axial stress became uniform to within 5 to 10 psi. A curve passing through these locations describes the limit of the effect of sidewall friction for the Case I problem. As mentioned above, the grout was considered welded to the steel in the analytical solution, and the boundary in Figure B.5 probably represents the most severe condition possible. Superimposed on the half section in Figure B.5 is the location of the GRT gage as tested. Note that the gage is clearly outside the zone affected by sidewall friction in a problem planned to maximize the region influenced by sidewall friction.

B.8 EFFECT OF GAGE IN THE GROUT

Case II considered the GRT gage as idealized by a piece of steel embedded in the grout. Since the gage is not entirely steel, this case is an upper bound approximation of the stiffness of the gage. The elements of steel and grout were considered welded. Figure B.6 shows a plot of the axial stress distribution across the specimen at an elevation directly above the gage. The circles indicate the axial stress distribution only for the grout without the gage from Case I The squares show the axial stress distribution with the steel gage in the grout. From the steel ring to 1.3 inches from the centerline, the axial stress distribution for the two cases is equal to $\pm$10 psi. The axial stress distribution in Case II then decreases as the gage is approached. At the gage/grout boundary, the vertical stress rises sharply. Over the gage face, the stress decreases and becomes uniform over the center section of the gage at a value about 5 percent greater than the applied stress

and the stress in the calculation where the gage was absent.

The axial stresses in the elements in the top of the steel gage are shown as triangles. Except at the gage edge, the stress distribution agrees favorably with the distribution in the overlying grout. The sharp rise at the edge is due to a stress concentration zone. Since the applied stress was 4,000 psi and the active portion of the gage is in the center half of its surface area, the distribution of axial stress over the gage indicates that the gage should overregister by approximately 5 percent.

B.9 EFFECT OF A VOID ABOVE THE GAGE

Cases III and IV considered the effect of a 20-mil-thick void directly above the gage face. Figure B.7 shows a plot of the axial stress distribution across the specimen for the void filled with water, Case III, and for the void filled with air, Case IV. The circles show the results for Case III. The distribution is approximately the same as that for Case II, grout over the gage. The stress distribution over the gage is nearly uniform. A perfectly uniform distribution would be expected for water, but it will be recalled that the code limitation required a nonzero G. The X's show the distribution within the top face of the steel gage; except at the gage edge, the stress is uniform. The results indicate that, for the case of a water-filled void over the gage, the gage should also overregister by approximately 5 percent.

The results for the case considering an air-filled void directly over the gage differed from the previously presented cases. The triangles in Figure B.7 show the axial stress distribution across the specimen in the layer of elements located at an elevation directly over the top gage face. The squares show the stress in the top layer of elements in the steel gage. The results indicate a dramatic underregistration of the gage (300 psi acting on the gage versus the 4,000 psi applied), a very high stress concentration at the edge of the gage, and a reduction in the effect of sidewall friction at the outer edge of the grout specimen.

Although the condition of an air void below the gage was not

considered, the results of Case IV may be used to approximate the stress distribution. The average axial stress in the grout elements directly below the gage was 2,600 psi. Because this problem was nearly symmetrical about a horizontal plane through the gage, it can be inferred that, had the air void been located under the gage, the stress on the top surface of the gage would have been lower than the applied pressure but not as low as that in Case IV.

B.10 SUMMARY AND CONCLUSIONS

A finite element computer code, WESTES, was used to determine the axial stress distribution within a half section of grout material surrounded by a steel ring. Four different conditions were considered: Case I was the steel ring and grout material; Case II included an embedded steel gage; Case III included the steel gage and a water-filled void above the gage; and Case IV included an air-filled void above the gage. In all cases, the grout material was considered welded to the steel ring and steel gage.

The results indicate that the zone of reduced stress caused by the effect of sidewall friction does not extend into the center portion of the specimen where the GRT gage is located. The results also show that, for the condition of the steel gage surrounded by grout and for the condition of a water-filled void over the gage, the gage should overregister the applied surface pressure by about 5 percent. For the condition of the air-filled void, the results indicate a registration of the gage of 300 psi for an applied surface pressure of 4,000 psi. The effect of the air void also seems to decrease the effect of the sidewall friction.

The conclusions based on the cases studied are as follows:

1. Sidewall friction could not have significantly prevented the applied surface pressure from reaching the embedded gage; therefore, the first hypothesis given in Section B.1 is not correct.

2. The axial stress distribution within the specimen is influenced by the embedment of a steel gage. Large stress concentrations occur at the edge of the gage.

3. The material located directly above (or below) a stress gage greatly affects the response of the gage: (1) A steel gage surrounded by a grout should tend to overregister axial stress applied to the grout surface; thus, the second hypothesis could explain those cases in which small overregistrations occurred. (2) A water-filled void above the gage should also cause an overregistration by the gage. (3) An air-filled void above the gage will prevent the applied axial stress from reaching the gage, thereby causing the gage to underregister. For the condition calculated, the gage would have registered only 300 psi for an applied surface pressure of 4,000 psi. It is felt that a void under the gage should also cause an underregistration, but not as great a one. Thus, an air-filled void could explain underregistration of the gage. Underregistration followed by proper registration later in the same test sequence could be explained by an air-filled void becoming filled with water as load application causes pore water migration within the specimen. The third hypothesis given in Section B.1, or the variation of it discussed in the preceding sentence, is the most consistent explanation with the observed test results and the code calculations presented herein. How such a void could form is not immediately clear, but a volume change of the grout during curing, a volume change of the gage due to the temperature changes caused by curing, or both could be responsible. Also, there may have been some air trapped in the mix during the pour. During the first few hours after grout preparation the bleed water which rose to the top of the specimen could have carried some trapped air with it. Some of this air could have been trapped under the gage.

4. It should be noted that the results of this investigation were based on simplified assumptions, such as no slip allowed between the grout and steel, and simplified material properties. The trends seen in the results, however, are reasonable and are believed to be indicative of the trend of actual response of a very stiff stress gage embedded in a grout material.

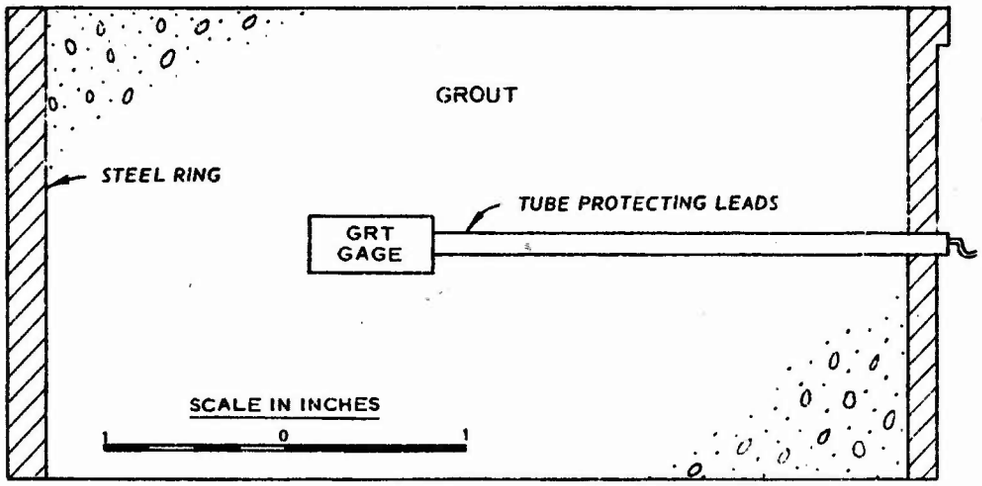

Figure B.1 Cross section of special grout specimen with embedded GRT gage.

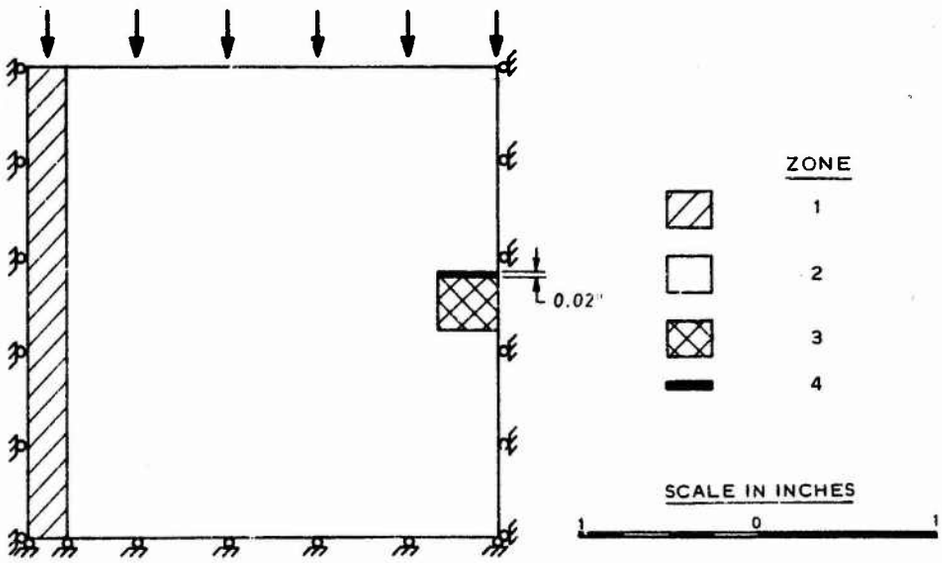

	CASE I	CASE II	CASE III	CASE IV
ZONE 1	STEEL	STEEL	STEEL	STEEL
ZONE 2	GROUT	GROUT	GROUT	GROUT
ZONE 3	GROUT	STEEL	STEEL	STEEL
ZONE 4	GROUT	GROUT	WATER	AIR

Figure B.2 Half section of grout and gage as idealized for finite element code.

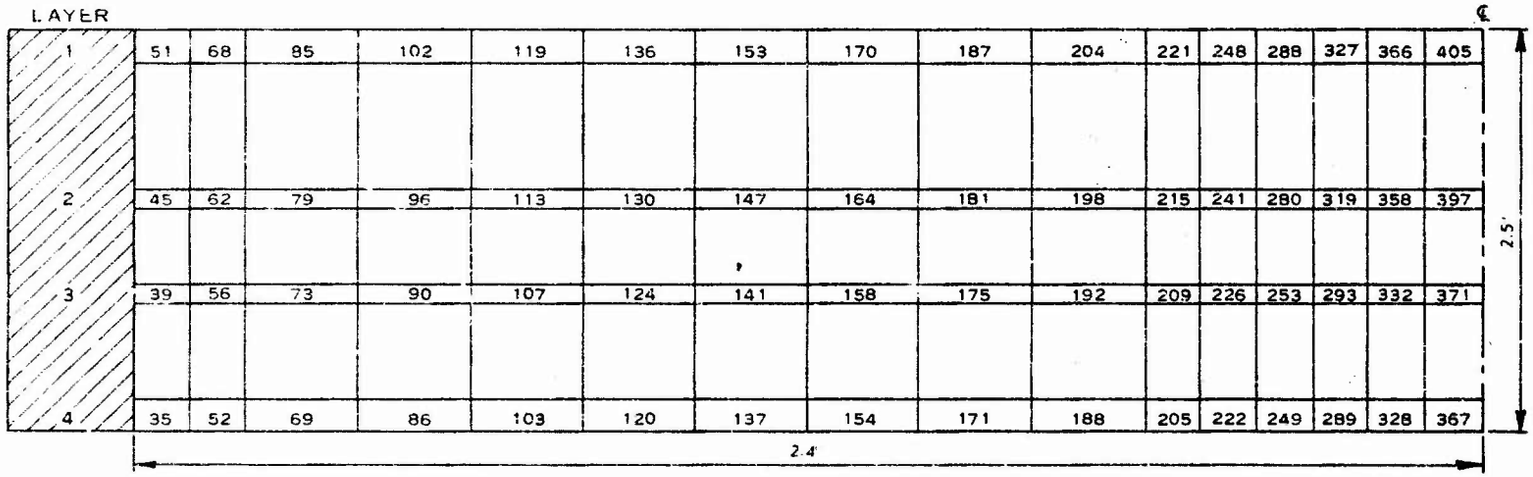

Figure B.3 Half section of grout specimen showing elements of interest.

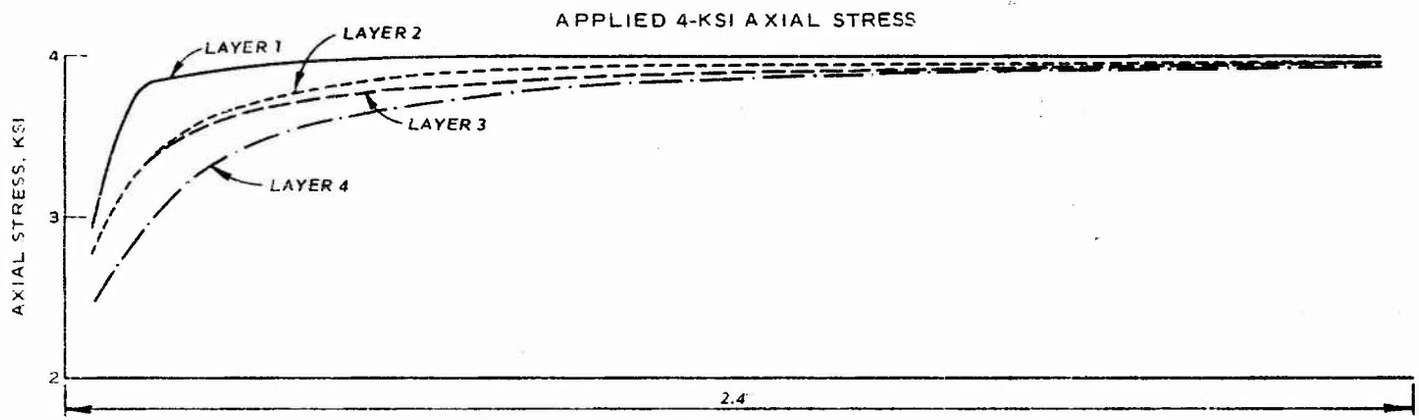

Figure B.4 Plot of axial stress versus location of elements showing axial stress distribution across specimen at four elevations.

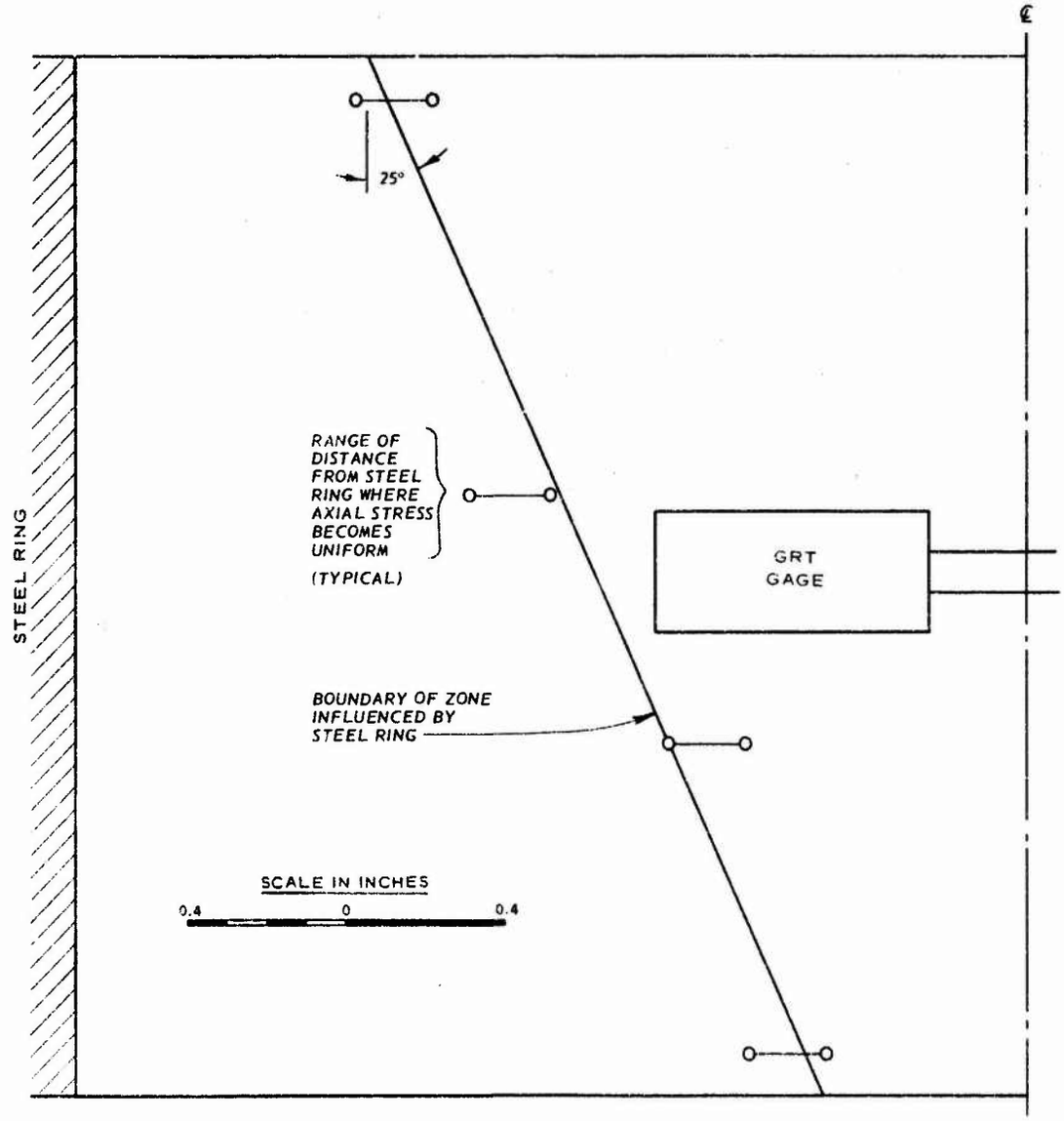

Figure B.5 Half section of specimen with actual location of GRT gage showing limit of sidewall friction on axial stress distribution across specimen.

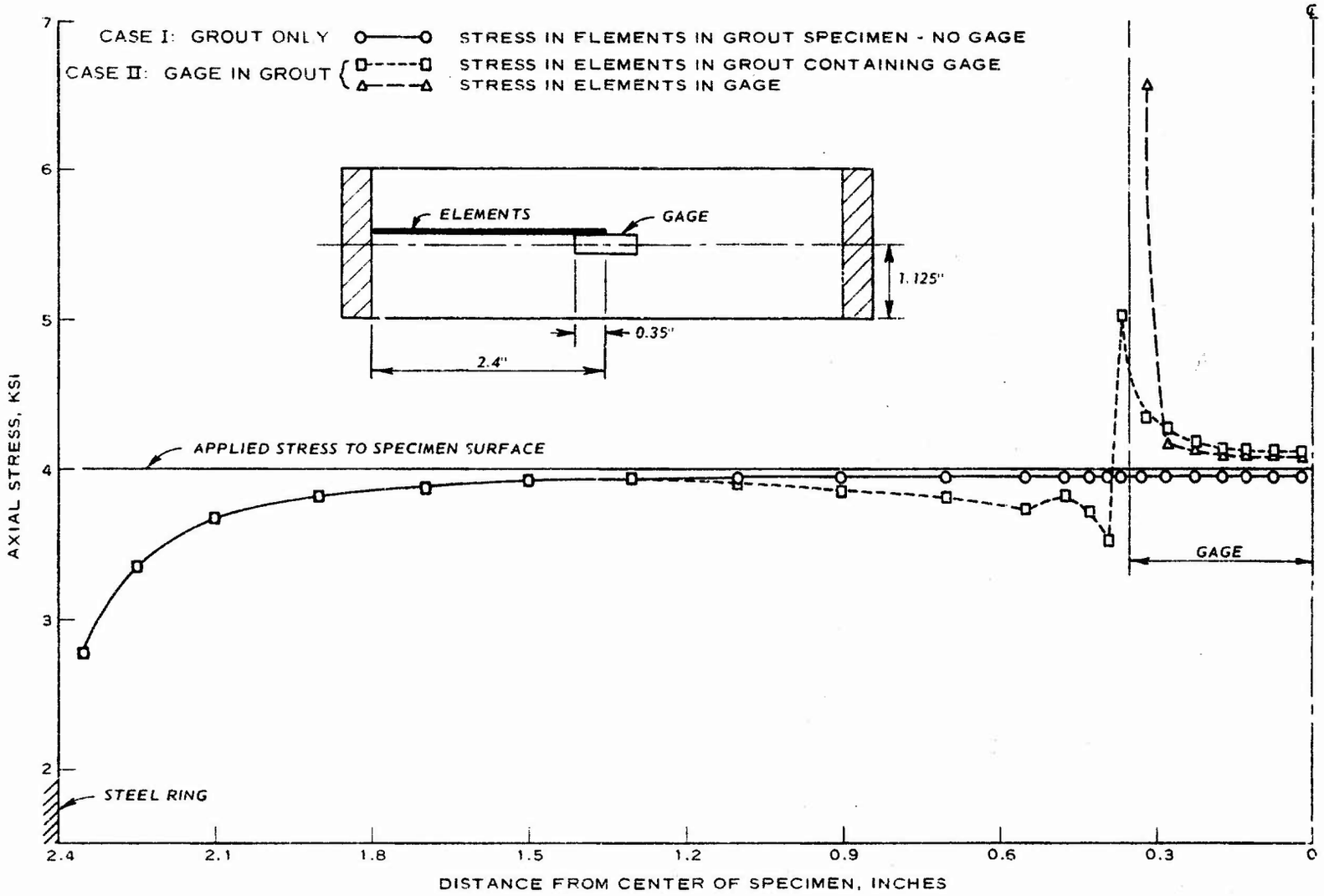

Figure B.6 Results of Cases I and II plotted as axial stress versus element location for elevation directly above gage.

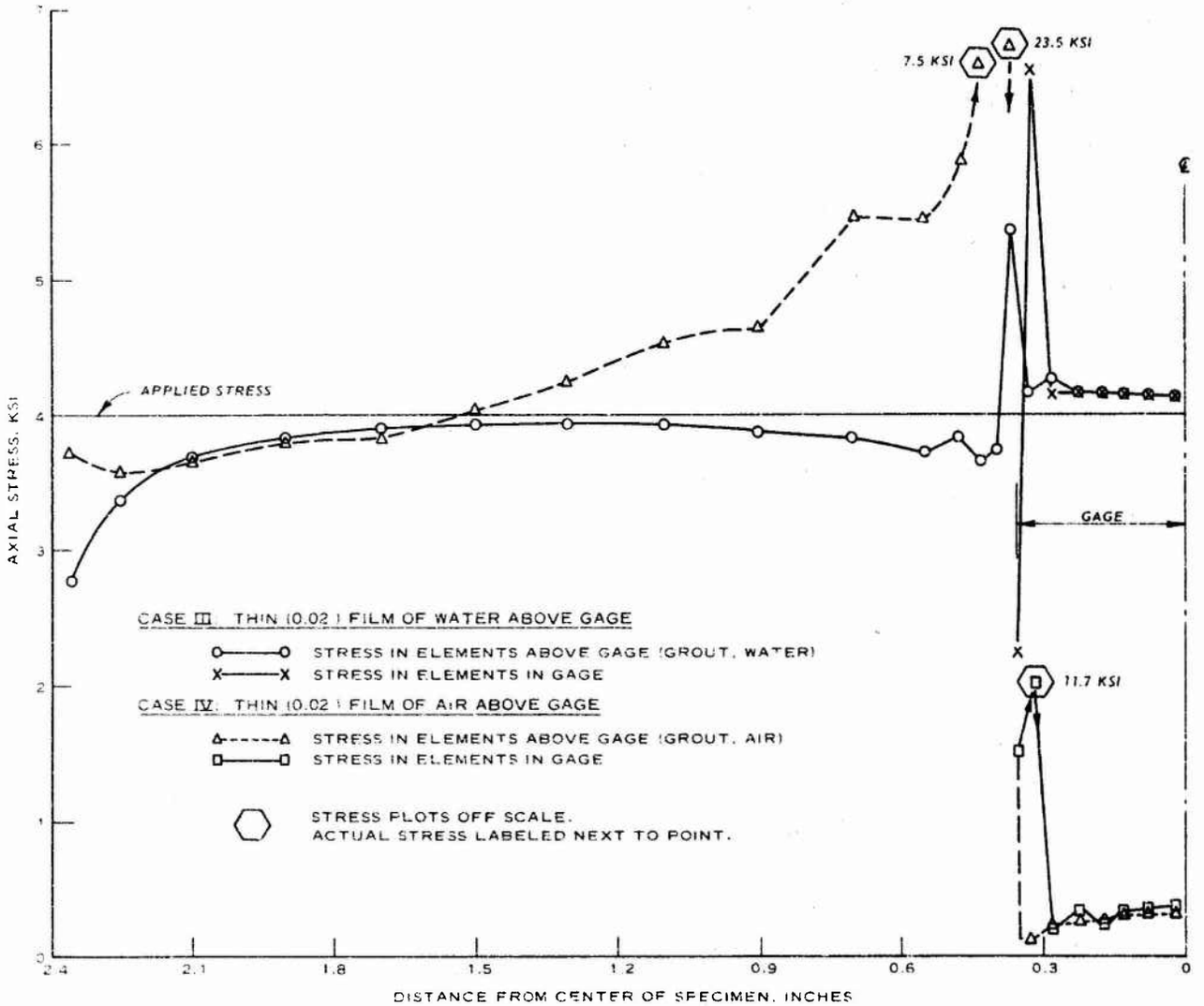

Figure B.7 Results of Cases III and IV plotted as axial stress versus element location for elevation directly above gage.

REFERENCES

1. P. F. Hadala; "Sidewall Friction Reduction in Static and Dynamic Small Blast Load Generator Tests"; Technical Report S-68-4, August 1968; U. S. Army Engineer Waterways Experiment Station, CE, Vicksburg, Mississippi; Unclassified.

2. N. Radhakrishnan; "Analysis of Stress-Strain Distribution in Triaxial Tests Using a Variable Moduli Model"; (in preparation); U. S. Army Engineer Waterways Experiment Station, CE, Vicksburg, Mississippi; Unclassified.

3. I. Nelson; "Investigation of Ground Shock Effects in Nonlinear Hysteretic Media, Modeling the Behavior of a Real Soil"; Contract Report S-68-1, Report 2, July 1968; U. S. Army Engineer Waterways Experiment Station, CE, Vicksburg, Mississippi; prepared by Paul Weidlinger, Consulting Engineer, under Contract No. DACA39-67-C-0048; Unclassified.